Parameterization of Size of Organic and Secondary Inorganic Aerosol for Efficient Representation of Global Aerosol Optical Properties

Haihui Zhu[1]*, Randall V. Martin[1,2], Betty Croft[2,1], Shixian Zhai[3], Chi Li[1], Liam Bindle[1], Jeffrey R. Pierce[4], Rachel Y.-W. Chang[2], Bruce E. Anderson[5], Luke D. Ziemba[5], Johnathan W. Hair[5], Richard A. Ferrare[5], Chris A. Hostetler[5], Inderjeet Singh[1], Deepangsu Chatterjee[1], Jose L. Jimenez[6], Pedro Campuzano-Jost[6], Benjamin A. Nault[7], Jack E. Dibb[8], Joshua S. Schwarz[9], Andrew Weinheimer[10]

[1] Department of Energy, Environmental & Chemical Engineering, Washington University in St. Louis, St. Louis, MO, USA

[2] Department of Physics and Atmospheric Science, Dalhousie University, Halifax, Nova Scotia, Canada

[3] Harvard John A. Paulson School of Engineering and Applied Sciences, Harvard University, Cambridge, MA, USA

[4] Department of Atmospheric Science, Colorado State University, Fort Collins, CO, USA

[5] NASA Langley Research Center, Hampton, VA, USA

[6] Cooperative Institute for Research in Environmental Sciences and Department of Chemistry, University of Colorado, Boulder, CO, USA

[7] Center for Aerosol and Cloud Chemistry, Aerodyne Research, Inc., Billerica, MA, USA

[8] Institute for the Study of Earth, Oceans, and Space, University of New Hampshire, Durham, NH, USA

[9] National Oceanic and Atmospheric Administration Chemical Sciences Laboratory, Boulder, CO, USA

[10] National Center for Atmospheric Research, Boulder, CO, USA

Correspondence: Haihui Zhu (haihuizhu@wustl.edu)

Abstract Accurate representation of aerosol optical properties is essential for modeling and remote sensing of atmospheric aerosols. Although aerosol optical properties are strongly dependent upon the aerosol size distribution, use of detailed aerosol microphysics schemes in global atmospheric models is inhibited by associated computational demands. Computationally efficient parameterizations for aerosol size are needed. In this study, airborne measurements over the United States (DISCOVER-AQ) and South Korea (KORUS-AQ) are interpreted with a global chemical transport model (GEOS-Chem) to investigate the variation in aerosol size when organic matter (OM) and sulfate-nitrate-ammonium (SNA) are the dominant aerosol components. The airborne measurements exhibit a strong correlation (r = 0.83) between dry aerosol size and the sum of OM and SNA mass concentration (M_{SNAOM}). A global microphysical simulation (GEOS-Chem-TOMAS) indicates that M_{SNAOM}, and the ratio between the two components ($\frac{OM}{SNA}$) are the major indicators for SNA and OM dry aerosol size. A parameterization of dry effective radius (R_{eff}) for SNA and OM aerosol is designed to represent the airborne measurements (R^2 = 0.74, slope = 1.00) and the GEOS-Chem-TOMAS simulation (R^2 = 0.72, slope = 0.81). When applied in the GEOS-Chem high-performance model, this parameterization improves the agreement between the simulated aerosol optical depth (AOD) and the ground-

measured AOD from the Aerosol Robotic Network (AERONET; R^2 from 0.68 to 0.73, slope from 0.75 to 0.96). Thus, this parameterization offers a computationally efficient method to represent aerosol size dynamically.

1 Introduction

Aerosol size has numerous effects on aerosol physical and chemical properties and further on atmospheric chemistry. Aerosol size-dependent heterogeneous chemistry affects gaseous oxidants that in turn affect production rates of aerosol components such as sulfate and secondary organic aerosol (Ervens et al., 2011; Estillore et al., 2016). Aerosol size also affects loss rates due to dry and wet deposition (Seinfeld and Pandis, 2016). Both direct and indirect aerosol radiative forcing are sensitive to aerosol size, as aerosol size affects the interaction between particles and radiation, and the water supersaturation ratio needed for a particle to be activated into a cloud droplet (Adams and Seinfeld, 2002; Faxvog and Roessler, 1978; Mishchenko et al., 2002; Emerson et al., 2020). The size dependence of aerosol extinction and scattering phase function also affects the retrieval of aerosol properties from satellites (Levy et al., 2013; Kahn et al., 2005; Jin et al., 2023). Aerosol size affects the fraction of particles that deposit in the body when breathing as well as location within the body where they deposit (Hinds and Zhu, 1999). An appropriate representation of aerosol size is essential for modeling aerosol composition and optical properties (Kodros and Pierce, 2017), interpreting satellite data (Levy et al., 2013; Kahn et al., 2005), studying climate processes (Twomey, 2007; Kellogg, 1980), and moving from aerosol exposure towards dose in health studies (Kodros et al., 2018).

The evolution of the aerosol size distribution is affected by various processes, such as nucleation, condensation, coagulation, and deposition. Nucleation events contribute to the number of particles in the nucleation mode (diameters less than about 10 nm) and thus tend to decrease the mean aerosol size for a population (Aalto et al., 2001). In polluted areas with high emission rates of aerosol precursors, mean aerosol size tends to increase by condensation and coagulation (Sakamoto et al., 2016; Sun et al., 2011). Dry and wet aerosol deposition have strong size dependencies due to competing physical processes (Emerson et al., 2020; Ruijrok et al., 1995; Reutter et al., 2009). The aerosol size distribution can be simulated using aerosol microphysical schemes, such as the TwO Moment Aerosol Sectional (TOMAS; Adams and Seinfeld, 2002) microphysics model, the Advanced Particle Microphysics (APM; Yu and Luo, 2009) model, the Global Model of Aerosol Processes (GLOMAP; Mann et al., 2010), and the Modal Aerosol Module (MAM4; Liu et al., 2016). These schemes have valuable prognostic capabilities; however, their computational cost has limited their use in Chemistry Climate Models (CCMs) or Chemical Transport Models (CTMs). For example, the wall clock time increases by about 2.5 times when APM is enabled in GEOS-Chem CTM relative to the bulk model (GCST et al., 2023). Only 3 of the 10 models that included aerosols, studied by the Atmospheric Chemistry and Climate Model Intercomparison Project, include online size-resolved aerosol microphysics, reflecting its computational cost and complexity (Lamarque et al., 2013; Liu et al., 2012; Szopa et al., 2013; Kodros and Pierce, 2017).

Methods are needed to better represent aerosol size in CCMs or CTMs without a microphysics scheme (referred to as bulk models). These bulk models usually use prescribed relationships to obtain size-resolved aerosol properties (Croft et al., 2005; Karydis et al., 2011; Zhai et al., 2021), which may insufficiently represent the temporal and spatial

variation (Kodros and Pierce, 2017). For example, in the GEOS-Chem CTM, a fixed dry aerosol geometric mean radius (R_g) is assumed for organic matter (OM) and sulfate-nitrate-ammonium (SNA), which is based on analysis of long-term aerosol composition and scattering measurements provided by the IMPROVE network across the continental U.S. (Latimer and Martin, 2019). However, subsequent analysis by Zhai *et al.* (2021) found that this aerosol size underestimated the aerosol mass scattering efficiency and the aerosol extinction coefficients during an aircraft campaign over South Korea (KORUS-AQ). Thus, neglect of aerosol microphysical processes that shape aerosol size distributions can be a significant source of uncertainty in aerosol optical properties in a CTM. A balance between computational cost and representativeness of aerosol size is needed. One option is to use models with size-resolved aerosol microphysics models to inform bulk models, such as was done for the parameterization of biomass burning aerosol size by Sakamoto *et al*. (2016).

Recent airborne measurements offer information to evaluate and improve the simulation of aerosol size. DISCOVER-AQ (Deriving Information on Surface Conditions from Column and Vertically Resolved Observations Relevant to Air Quality) was a multi-year campaign over four U.S. cities that provides 3-D resolved measurements of atmospheric gas composition, aerosol composition, size distribution, and optical properties (Choi et al., 2020; Sawamura et al., 2017; Chu et al., 2015). KORUS-AQ (the Korea-United States Air Quality Study) offers similar measurements in a different environment with higher aerosol mass loadings (Choi et al., 2020; Zhai et al., 2021; Nault et al., 2018; Jordan et al., 2020).

To study the global variation in aerosol size, we explore airborne measurements from DISCOVER-AQ and KORUS-AQ, as well as output from the GEOS-Chem-TOMAS microphysics model. We focus on OM and SNA, which dominate fine aerosol composition in populated areas (Weagle et al., 2018; Geng et al., 2017; Meng et al., 2019; Van Donkelaar et al., 2019; Li et al., 2017). The driving factors for variation in aerosol size are examined. A parameterization of aerosol size using these driving factors is proposed. This parameterization is then applied to a GEOS-Chem high-performance model bulk simulation for global aerosol optical depth (AOD), which is evaluated by ground-measured AOD from the Aerosol Robotic Network (AERONET).

2 Observations and Models

2.1 Observations

2.1.1 Aircraft measurements

We examine airborne measurements from two NASA campaigns, DISCOVER-AQ and KORUS-AQ. DISCOVER-AQ includes four deployments in Maryland (MD), California (CA), Texas (TX), and Colorado (CO). KORUS-AQ is an international cooperative field study program conducted in South Korea (KO), sponsored by NASA and the South Korean government through the National Institute of Environmental Research. The year as well as the date and altitude ranges of each deployment are in Table 1.

Table 1. Temporal and spatial coverage of each aircraft deployment

Campaign	Year	Date Range	Altitude from surface
MD	2011	07/01-07/29	0 to 5 km
TX	2013	09/04-09/29	0 to 5 km
CA	2013	01/16-02/06	0 to 4 km
CO	2014	07/17-08/10	0 to 6 km
KO	2016	05/02-06/11	0 to 8 km

Measurements used in this study include aerosol composition, ambient aerosol extinction, aerosol number size distribution, gas tracer species, and meteorological data. Measurement methods are listed in Table 2. Measured aerosol mass is converted from standard to ambient condition before analysis using ambient temperature and pressure. We use OM directly measured during KORUS-AQ. We use water soluble organic carbon (OC) and a parameterized ratio between OM and OC (Philip et al., 2014) to calculate OM for DISCOVER-AQ. The parameterized OM is evaluated with KORUS-AQ data, and overall consistency is found (Figure A1; Appendix A). For both campaigns, dust concentration is derived from Ca^{2+} and Na^{+} assuming non-sea salt Ca^{2+} accounts for 7.1% of dust mass (Shah et al., 2020):

$$Dust = \frac{\left([Ca^{2+}] - 0.0439\frac{[Na^{+}]}{2}\right)}{0.071} \quad \text{Eqn. (1)}$$

Sea salt is calculated from measured Na^{+} following previous studies (Remoundaki et al., 2013; Malm et al., 1994; Snider et al., 2016). The crustal component is removed by subtracting 10 % of $[Al^{3+}]$ (Remoundaki et al., 2013). A 2.54 scalar is applied to $[Na^{+}]_{ss}$ to account for $[Cl^{-}]$ (Malm et al., 1994):

$$Sea\ Salt = 2.54([Na^{+}] - 0.1[Al^{3+}]) \quad \text{Eqn. (2)}$$

Effective radius (R_{eff}) (Hansen and Travis, 1974), defined as the area-weighted mean radius of a particle population, is used as a surrogate for aerosol size:

$$R_{eff} = \frac{\int r\pi r^2 n(r)dr}{\int \pi\, r^2 n(r)dr} \quad \text{Eqn. (3)}$$

Measurement data are screened for dust influence by excluding data with the sum of SNA and OM (M_{SNAOM}) < 4 × dust mass.

Table 2. Aircraft observations used in this study[*]

Variables	DISCOVER-AQ	KORUS-AQ
Bulk aerosol ionic composition	IC-PILS [a]	SAGA [b]
Sub-micron non-refractory aerosol composition	TOC-PILS [c]	HR-ToF-AMS [d]
Refractory black carbon concentration	SP2 [e]	
Dry aerosol size distribution	UHSAS [f] or LAS [g]	LAS [g]
Aerosol extinction profile at 532 nm	HSRL [h]	
NO_2	4-Channel Chemiluminescence Instrument [i]	
Relative humidity (RH)	DLH [j]	

[*] Adapted from Zhai et al. (2021)

[a] Ion Chromatography Particle-Into-Liquid Sampler, with a 1.3 μm inlet cutoff aerodynamic diameter (Lee et al., 2003; Hayes et al., 2013).

[b] Soluble Acidic Gases and Aerosol (SAGA) instrument (Dibb et al., 2003). The cutoff aerodynamic diameter of the inlet is around 4 μm (McNaughton et al., 2007).

[c] Water-soluble organic carbon Particle-Into-Liquid Sampler, with a 1 μm inlet cutoff diameter at 1 atmosphere ambient pressure (Sullivan et al., 2019; Timonen et al., 2010).

[d] University of Colorado Boulder High-Resolution Time-of-Flight Aerosol Mass Spectrometer (HR-ToF-AMS) with a 1 μm inlet cutoff diameter (Nault et al., 2018; Guo et al., 2021; Canagaratna et al., 2007).

[e] Single-Particle Soot Photometer (SP2), measuring refractory black carbon with a volume equivalent diameter of 100-500 nm (Lamb et al., 2018; Schwarz et al., 2006).

[f] Particles with mobility diameters between 60 to 1000 nm can be measured by Ultra-High Sensitivity Aerosol Spectrometer (UHSAS), which illuminates particles with a laser and relate the single-particle light scattering intensity and count rate measured over a wide range of angles to the size-dependent particle concentration (Moore et al., 2021). Particles in the sample are dried to less than 20 % RH.

[g] Particles between 100 to 5000 nm measured by Laser Aerosol Spectrometer (LAS, TSI model 3340). The principle of LAS is the same as that of UHSAS, but with a different laser wavelength (1054 nm for the UHSAS and 633 nm for the LAS) and intensity (about 100 times higher for the UHSAS). These differences affect how the instrument sizes non-spherical or absorbing aerosols (Moore et al., 2021). Particles in the sample are dried to less than 20 % RH.

[h] NASA Langley airborne High Spectral Resolution Lidar (HSRL) (Hair et al., 2008).

[i] National Center for Atmospheric Research (NCAR) 4-Channel Chemiluminescence Instrument (Weinheimer et al., 1993)

[j] NASA Diode Laser Hygrometer (DLH) (Podolske et al., 2003).

2.1.2 AERONET AOD

We use ground-based AOD observations to evaluate our parameterization and simulated AOD. The Aerosol Robotic Network (AERONET) is a worldwide network that provides long-term sun photometer measured AOD, and is conventionally considered as the ground truth for evaluating model-simulated (Zhai et al., 2021; Meng et al., 2021; Jin et al., 2023) or satellite-retrieved AOD (Levy et al., 2013; Wang et al., 2014a; Kahn et al., 2005; Lyapustin et al., 2018). We use the Version 3 Level 2 database, which includes an improved cloud screening algorithm (Giles et al., 2019). AOD at 550 nm wavelength, interpolated based on the local Ångström exponent at 440 and 670 nm channels, is used in this study. For each site, we use data for the year 2017, excluding months with less than 20 days of measurements and excluding sites with less than 4 months of observations.

2.2 GEOS-Chem simulation

We interpret the aircraft observations with the GEOS-Chem chemical transport model (www.geos-chem.org, last access: 30 October 2022). GEOS-Chem is driven by offline meteorological data from the Goddard Earth Observing System (GEOS) of the NASA Global Modeling and Assimilation Office (Schubert et al., 1993). We use the high-performance implementation of GEOS-Chem (GCHP) (Eastham et al., 2018; Bindle et al., 2021) to examine the effect of variation in aerosol size on AOD. We also use the TOMAS microphysical scheme, coupled with the standard GEOS-Chem implementation (GEOS-Chem Classic), to explicitly resolve aerosol microphysics. The bulk and the microphysics simulations share common emissions and chemical mechanisms. They are both conducted for the year 2017 and driven by MERRA-2 meteorological fields.

The GEOS-Chem aerosol simulation includes the sulfate-nitrate-ammonium system (Fountoukis and Nenes, 2007; Park, 2004), primary and secondary carbonaceous aerosols (Park et al., 2003; Wang et al., 2014b; Marais et al., 2016; Pye et al., 2010), sea salt (Jaeglé et al., 2011), and mineral dust (Fairlie et al., 2007). The primary emission data are from the Community Emissions Data System ($CEDS_{GBD\text{-}MAPS}$; McDuffie et al., 2020). Dust emission inventories include updated natural dust emission (Meng et al., 2021b), and anthropogenic fugitive, combustion, and industrial dust (AFCID; Philip et al., 2017). Resolution-dependent soil NO_x, sea salt, biogenic VOC, and natural dust emissions are calculated offline at native meteorological resolution to produce consistent emissions across resolution (Weng et al., 2020; Meng et al., 2021b). Biomass burning emissions use the Global Fire Emissions Database, version 4 (GFED4) (Van Der Werf et al., 2017). We estimate organic matter (OM) from primary organic carbon using the same OM/OC parameterizations as applied for DISCOVER-AQ (Philip et al., 2014; Canagaratna et al., 2015). Dry and wet deposition follows Amos *et al.* (2012), with a standard resistance-in-series dry deposition scheme (Wang et al., 1998). Wet deposition includes scavenging processes from convection and large-scale precipitation (Liu et al., 2001).

Global relative humidity dependent aerosol optical properties are based on the Global Aerosol Data Set (GADS) (Kopke P., 1997; Martin et al., 2003) with updates for SNA and OM (Latimer and Martin, 2019), mineral dust (Zhang et al., 2013), and absorbing brown carbon (Hammer et al., 2016). In the current GEOS-Chem model, the SNA and

OM R_{eff} of particular interest here are based on co-located measurements of aerosol scatter and mass from the IMPROVE network at U.S. national parks over the period 2000-2010, together with a κ-Kohler framework for aerosol hygroscopicity (Kreidenweis et al., 2008) as implemented by Latimer and Martin (2019). Aerosol extinction is calculated as the sum of extinction from each aerosol component with aerosol optical properties listed in Table A1, as described in Appendix A2.

A global GCHP simulation (Eastham et al., 2018) version 13.0.0 (DOI: 10.5281/zenodo.4618180) that includes advances in performance and usability (Martin et al., 2022), is conducted on a C90 cubed-sphere grid corresponding to a horizontal resolution of about 100 km, with a spin-up time of 1 month.

The TOMAS microphysics scheme, coupled with the GEOS-Chem simulation, conserves aerosol mass, and tracks particles with diameters from approximately 1 nm to 10 μm (Adams and Seinfeld, 2002). Microphysical processes in TOMAS include nucleation, condensation, evaporation, coagulation, and wet and dry deposition (Adams and Seinfeld, 2002). Nucleation in TOMAS follows a ternary scheme (sulfuric acid, ammonia, and water) when ammonia mixing ratios are greater than 0.1 ppt; otherwise, a binary nucleation scheme is used (Napari et al., 2002). The nucleation rate is scaled by 10^{-5} to better match the observations (Westervelt et al., 2013). The condensation and evaporation algorithm is based on a study from Tzivion *et al.* (1989), including interaction with secondary organic aerosol (D'Andrea et al., 2013). Interstitial coagulation in clouds is also included (Pierce et al., 2015).

For each size bin, TOMAS tracks the mass and number of sulfate, sea salt, black carbon, OC, dust, and water. Primary sulfate emissions have 2 lognormal modes: 15% of the mass with a number median diameter (NMD) of 10 nm and geometric standard deviation (σ) of 1.6 and the remainder with a NMD of 70 nm and σ of 2 (Adams and Seinfeld, 2003). The size of emitted carbonaceous particles varies depending on the source: those produced by fossil fuel have a NMD of 30 nm and σ of 2, while biofuel and biomass burning particles are emitted with a NMD of 100 nm and σ of 2 (Pierce et al., 2007). Meteorology and most of the emissions in GEOS-Chem-TOMAS follow the bulk simulation, except that online schemes are used for dust (Zender et al., 2003) and sea salt (Jaeglé *et al.* 2011).

The GEOS-Chem-TOMAS (version 13.2.1. DOI: 10.5281/zenodo.5500717) is used to provide insights into global scale aerosol size variation and the driving factors. For computational feasibility, a one-year global simulation is conducted with a horizontal resolution of 4º × 5º and 47 vertical layers from surface to 0.01 hPa. The spin-up time is 1 month. Aerosols are tracked in 15 size bins with particle diameters ranging from about 3 nm to 10 μm. We also conducted a 2º × 2.5º simulation for October to evaluate the sensitivity of our conclusions to the resolution of the aerosol microphysics simulation.

3 Development of a Parameterization of Aerosol Size

We first examine the aircraft measurements for insight into the observed variation in aerosol size. Then we apply the size-resolved GEOS-Chem-TOMAS model to extend our analysis to the global scale and identify driving factors of aerosol size. We subsequently develop and test a parameterization of aerosol size for use in bulk models.

3.1 Observed variation in aerosol size

Figure 1 shows the daily-mean dry effective radius from DISCOVER-AQ and KORUS-AQ as a function of aerosol mass. Aerosol size, in terms of dry R_{eff}, ranges from 90 nm to 179 nm for DISCOVER-AQ, which is generally smaller than for KORUS-AQ that ranges from 135 nm to 174 nm. M_{SNAOM} from DISCOVER-AQ (1.4 μg/m^3 to 27.4 μg/m^3) is also generally less than that from KORUS-AQ (5.5 μg/m^3 to 33.2μg/m^3). A strong correlation (r = 0.83) between aerosol size and M_{SNAOM} is evident. R_{eff} from KORUS-AQ is less sensitive to M_{SNAOM} (slope = 1.23) compared to DISCOVER-AQ (slope = 3.57). The relatively large particle size at low mass concentration during KORUS-AQ might reflect the influence of aged aerosol transported from upwind (Jordan et al., 2020; Zhai et al., 2021; Nault et al., 2018).

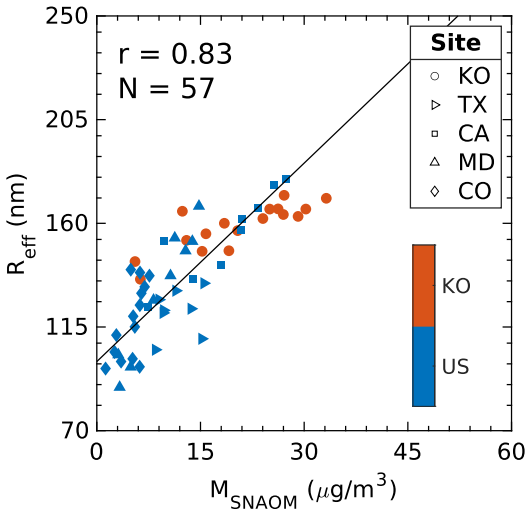

Figure 1. Airborne measurements of dry effective radius (R_{eff}) versus the sum of SNA and OM mass (M_{SNAOM}) for DISCOVER-AQ (Maryland is abbreviated as MD, California as CA, Texas as TX, Colorado as CO) and for KORUS-AQ (KO) campaigns. Each point represents a daily average for the entire flight profile. Only data with M_{SNAOM} > 4 × Dust mass is used.

The positive relationship between dry aerosol size and mass of SNA and OM reflects the roles of emission, condensation, and coagulation in simultaneously increasing aerosol size and mass. This general tendency is also observed by many other studies (e.g., Sakamoto et al., 2016; Rodríguez et al., 2007; Sun et al., 2012; Bahreini et al., 2003) despite variable aerosol sources and growth mechanisms. In cities, the joint increases in aerosol size and mass are usually attributable to anthropogenic emissions and condensation (Tian et al., 2019; Sun et al., 2011; Huang et al., 2013). In remote areas, biomass burning shifts the particle size distribution toward larger radii due to high emission rates and coagulation in plumes (Rissler et al., 2006; Ramnarine et al., 2019) that, for example, increase both aerosol size and mass from the wet season to the dry season in Amazonia (Rissler et al., 2006; Andreae et al., 2015). The positive relationship between aerosol size and mass suggests the possibility of using aerosol mass as a predictor of R_{eff}.

We examine the ability of the GEOS-Chem bulk model to reproduce the observed extinction. The top panel of Figure 2 compares the measured aerosol extinction profiles to calculated aerosol extinction profiles using default R_{eff}. Details about the calculation are described in Appendix A2. Both measured and calculated extinction profiles exhibit increasing extinction toward the surface associated with increasing aerosol mass concentrations. However, biases are apparent for both DISCOVER-AQ and KORUS-AQ. The R_{eff} from KORUS-AQ shown in Figure 1 have a mean value of 164 nm, larger than the value of 101 nm inferred by Latimer & Martin (2019) based on measurements of aerosol scatter and mass by the U.S. IMPROVE network. This bias was previously noted by Zhai *et al.* (2021). The mean R_{eff} from DISCOVER-AQ of 138 nm is also larger than the inferred value. This likely reflects representativeness differences since the DISCOVER-AQ deployments focused on major urban areas during months of high aerosol loadings, while the IMPROVE measurements were at national parks throughout the year. The middle panel shows the calculated extinction using the measured aerosol size distribution. Applying the measured aerosol size distribution addresses most discrepancies between the calculated and measured aerosol extinction profile for both KORUS-AQ and DISCOVER-AQ. The corresponding discrepancies in AOD estimation also significantly decreased (from 0.09 to 0.03 for DISCOVER-AQ and from 0.17 to 0.02 for KORUS-AQ). The reduced discrepancies support the conclusions from Zhai *et al.* (2021) that the GEOS-Chem aerosol size is underestimated for KORUS-AQ and motivate parameterization of R_{eff} for efficient representation of aerosol size for global scale aerosol modeling.

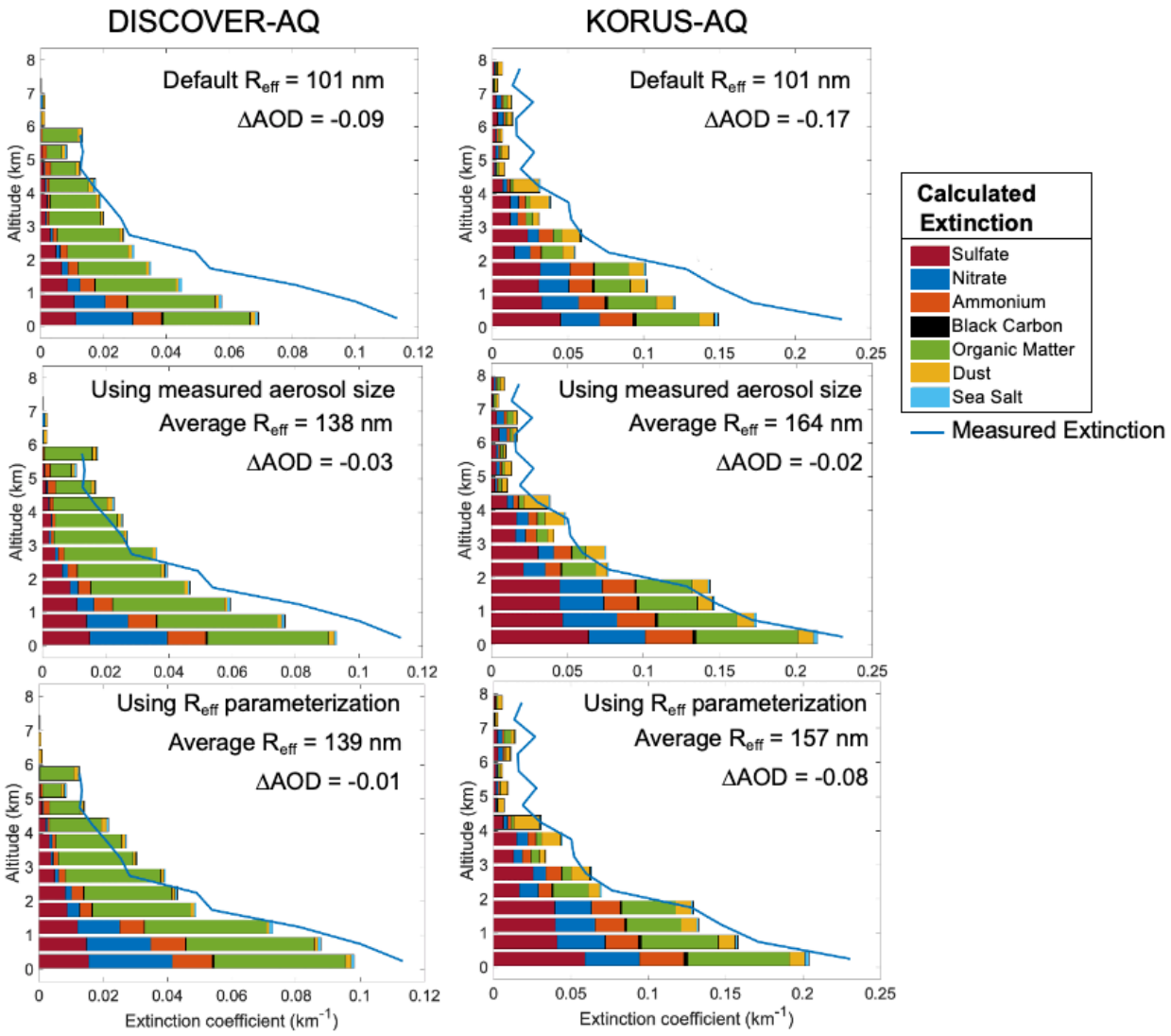

Figure 2. Aerosol extinction profile for the DISCOVER-AQ and KORUS-AQ aircraft campaigns. Blue lines are the measured extinction profiles. Horizontal bars are calculated extinction using (top) default GEOS-Chem R_{eff}, (middle) measured R_{eff}, and (bottom) parameterized R_{eff} (described in Section 3.3), together with measured aerosol composition and RH. The aerosol extinction calculation is described in Appendix A.

3.2 Driving factors

Given the strong positive correlation of aerosol mass with aerosol size, we further examine this relationship globally using GEOS-Chem coupled with the TOMAS aerosol microphysics scheme. To focus on areas that are dominated by SNA and OM, we only include grid boxes with M_{SNAOM} > 90% of the aerosol mass. Inspection of the GEOS-Chem-TOMAS size distribution across continental regimes reveals a general tendency for the distribution to shift toward smaller sizes as R_{eff} decreases and toward larger sizes as R_{eff} increases, thus supporting the use of the single summary statistic of R_{eff} for aerosol size. The top panel of Figure 3 shows the geographic distribution of annual mean surface layer dry R_{eff} for grid boxes that meet the criterion. Among the areas of interest, biomass burning regions of Central

Africa, South America, and boreal forests of North America exhibit the highest surface R_{eff} of about 180 nm. Industrial areas such as East Asia and South Asia also exhibit high R_{eff} of about 130 nm, given an abundance of particle emissions and gaseous precursors. The lowest surface R_{eff} of about 80 nm is found in North America, where aerosol mass concentrations are low.

The middle panel of Figure 3 shows the simulated M_{SNAOM} from GEOS-Chem-TOMAS. Enhanced M_{SNAOM} concentrations of over 40 $\mu g/m^3$ are apparent over East Asia and South Asia, reflecting intense anthropogenic emissions. Another M_{SNAOM} hotspot can be seen in Central Africa, driven by biomass burning during the dry season (Van Der Werf et al., 2017; McDuffie et al., 2021) and sometimes exacerbated by anthropogenic emissions (Ngo et al., 2019). Moving from North America to Europe, and then to Asia (defined by boxes in the middle panel), M_{SNAOM} concentrations exhibit a generally increasing tendency (mean value of 11, 17, and 25 $\mu g/m^3$, respectively), consistent with the R_{eff} tendency (mean value of 124, 133, and 136 nm, respectively) in the top panel and aligning with the relationship between aircraft measurements over the U.S. and South Korea.

However, in South America, where R_{eff} is among the highest, M_{SNAOM} is relatively low. This discrepancy motivates the search for other factors, such as aerosol composition, that are associated with aerosol size. In South America, aerosol mass is mostly from natural sources, particularly biomass burning during the dry seasons. R_g for a particle population from biomass burning ranges from 60 nm to 170 nm (Rissler et al., 2006; Reid et al., 2005; Janẗall et al., 2010), usually larger than that of primary sulfate aerosol (5 to 35 nm) (Whitey, 1978; Plaza et al., 2011). Therefore, the relative abundance of OM in the total M_{SNAOM} can serve as another predictor of R_{eff}. The bottom panel of Figure 3 shows the ratio between OM and SNA mass. In addition to the Amazon basin, the biomass burning regions of Central Africa and boreal forests in Asia and North America are all areas with high OM mass fractions, which contribute to their high R_{eff}.

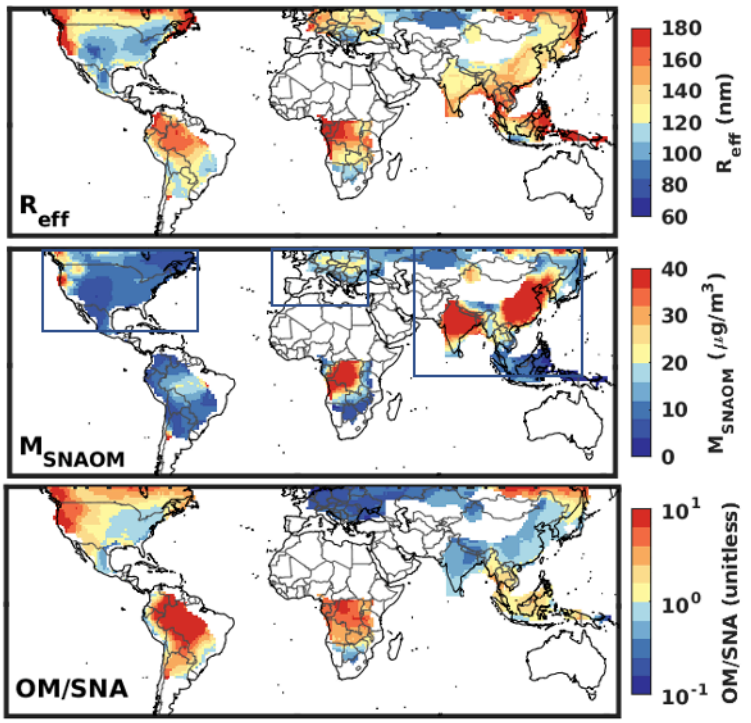

Figure 3: Geographic distribution of GEOS-Chem-TOMAS-simulated annual mean surface layer aerosol properties; (top) R_{eff} when M_{SNAOM} > 90% of aerosol mass, (middle) the sum of SNA and OM mass (M_{SNAOM}), and (bottom) OM/SNA.

3.3 Parameterization and evaluation

We use Multiple Linear Regression (MLR) to derive a parameterization of dry R_{eff} for SNA and OM as a function of M_{SNAOM} and OM/SNA. We sample the GEOS-Chem-TOMAS simulation for locations dominated by M_{SNAOM} (> 90%). We include all qualified data (8,569 grid boxes) from the planetary boundary layer (PBL) to focus on this region, while randomly sample 0.5% of simulations in the free troposphere (217,772 grid boxes) to allow the influence of remote regions in the training set. The reason for focusing on the PBL is twofold. First, the PBL generally has the highest aerosol loading that largely determines the columnar mass and AOD (Koffi et al., 2016; Zhai et al., 2021; Tian et al., 2019). Second, the PBL is the domain where most model-measurement difference exists (Figure 2, top panel).

Taking the logarithm of R_{eff} and the logarithm of the two predictors facilitates linear relationships for regression, which yields the initial parameterization

$$R_{eff} = 78.3 M_{SNAOM}^{0.20} \left(\frac{OM}{SNA}\right)^{0.065} \quad \text{Eqn. (4)}$$

where R_{eff} has units of nm, M_{SNAOM} has units of μg/m^3, and OM/SNA is unitless. The R_{eff} parameterization is driven primarily by the mass of SNA and OM, modulated by the ratio of OM to SNA. This equation well represents the variation of R_{eff} during the aircraft campaigns with an R^2 of 0.74 (Figure B1, top left). The slope below unity (0.90)

likely reflects the effect of coarse model resolution, which dilutes the particle or precursor concentration in turn reducing condensation and coagulation growth (AboEl-Fetouh et al., 2022; Ramnarine et al., 2019; Sakamoto et al., 2016). Adjustment to this parameterization to account for these effects and align the slope with the airborne measurements rather than the model results in a final parameterization of

$$R_{eff} = 87.0 M_{SNAOM}^{0.20} \left(\frac{OM}{SNA}\right)^{0.065} \quad \text{Eqn. (5)}$$

Figure 4 shows the distribution of dry R_{eff} based on GEOS-Chem-TOMAS and Eqn. (5). Circles in Figure 4 show the mean values of the sampled GEOS-Chem-TOMAS simulated R_{eff} as a function of simulated M_{SNAOM} concentrations, ranging from 0.02 to 102 μg/m^3, and OM/SNA ranging from 0.13 to 55. Simulated R_{eff} extends from 15 nm when both M_{SNAOM} and OM/SNA are low (0.09 μg/m^3 and 1.3, respectively), up to 282 nm when M_{SNAOM} and OM/SNA are high (about 44 μg/m^3 and 14 respectively). The background color indicates our parameterized R_{eff}. A high degree of consistency exists between the parameterized R_{eff} and simulated R_{eff}, especially in the free troposphere where large gradients in R_{eff} exist, with overall for the troposphere an R^2 of 0.72, and a slope of 0.81 (Figure B1, bottom right). At the lower end of R_{eff}, the agreement between simulation and the parameterization can also be found in Figure B1, which shows that the small R_{eff} are reproduced by the parameterization. Despite the overall consistency, a few differences exist. When aerosol mass concentration is high, the parameterization tends to yield a higher R_{eff} than in the GEOS-Chem-TOMAS simulation, since the adjustment using aircraft measurements led to 11% increase in R_{eff}. At M_{SNAOM} near 10 μg/m^3 and OM/SNA near 10, the simulation indicates higher R_{eff} than the parameterization, reflecting dilution downwind of biomass burning that reduces the aerosol mass concentration but has less influence on particle size in GEOS-Chem-TOMAS (Park et al., 2013; Rissler et al., 2006; Sakamoto et al., 2016). A 10-20% underestimation in the parameterization at low OM/SNA reflects the advection and dilution downwind of urban areas and in the free troposphere (Yue et al., 2010; Asmi et al., 2011). Evaluation of our parameterization versus the GEOS-Chem-TOMAS simulation of 2º × 2.5º for October yields similar results but explains an additional 14% of the variance in simulated R_{eff}, providing additional evidence of the fidelity of the parameterization.

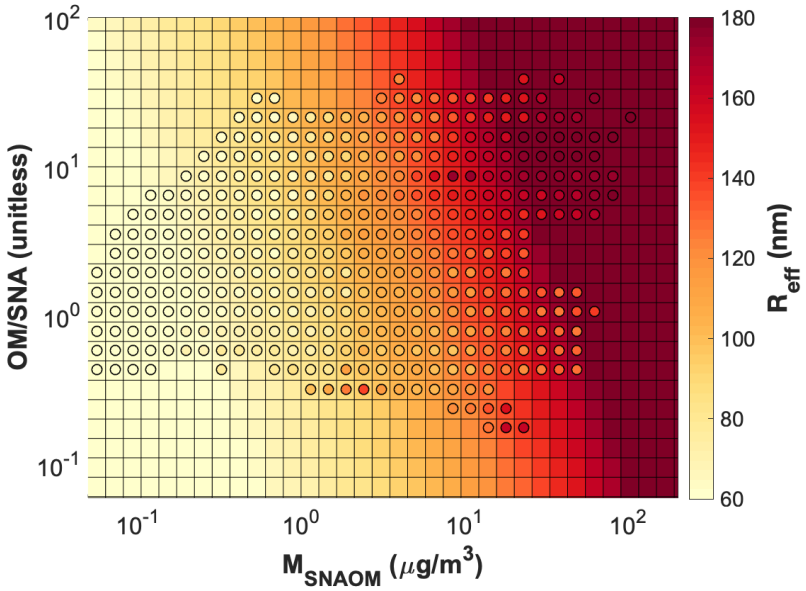

321

322 **Figure 4. Dry R_{eff} as a function of M_{SNAOM} and OM/SNA when SNA and OM are dominant (>90%). Each**
323 **circle represents the mean value of the GEOS-Chem-TOMAS simulated R_{eff} in each bin. Background color**
324 **indicates the parameterized R_{eff}.**

325 When applied to the airborne measurements, this parameterization only slightly overestimates the measured R_{eff} from
326 DISCOVER-AQ (139 nm vs. 138 nm) and slightly underestimates R_{eff} from KORUS-AQ (157 nm vs. 164 nm).
327 Discrepancies between calculated and measured extinction from aircraft campaigns are largely reduced (Figure 2,
328 bottom panel) with AOD biases of 0.01 and 0.08 for DISCOVER-AQ and KORUS-AQ, respectively. Minor
329 differences are still present in aerosol extinction above 4 km for KORUS-AQ, but a physical explanation remains
330 elusive since the calculated extinction is biased even if measured aerosol size and composition are used; instrument
331 uncertainties may play a role. Nonetheless, effects on columnar AOD from these disagreements aloft are minor (<5%).

332 We then apply Eqn. (5) to a GEOS-Chem bulk simulation to calculate R_{eff} and AOD. The top panel of Figure 5 shows
333 the annual mean dry R_{eff} for surface SNA and OM aerosol. The parameterized R_{eff} is usually higher than the default
334 value of about 100 nm in GEOS-Chem over land, and lower than that over the ocean, with a normalized root mean
335 square deviation (NRMSD) of 43.8%. The parameterized R_{eff} is the highest in biomass burning regions in South
336 America and Central Africa, as well as industrial regions in Asia, similar to the pattern found in the GEOS-Chem-
337 TOMAS simulation. The parameterized R_{eff} and its horizontal variation diminish with altitude (Figure B2), with the
338 mean R_{eff} of 85 nm at the surface decreasing by 18.8% to 69 nm at about 5 km. By design, the parameterization has
339 little effect in regions and seasons where and when M_{SNAOM} is not dominant, since the parameterization only affects
340 R_{eff} of SNA and OM.

341 The middle panel of Figure 5 shows the simulated AOD, with the corresponding difference between the base
342 simulation and the updated simulation in the bottom panel. To accommodate the parameterized R_{eff}, a look-up table
343 with a wide range of R_{eff} (0.02 μm to 1.7 μm) and the corresponding extinction efficiencies for OM and SNA is created

based on Mie Theory (Mishchenko et al., 2002, 1999). This update generally increases aerosol mass scattering by increasing the mass extinction efficiency, in turn, increasing AOD over regions with strong anthropogenic sources, such as East Asia (by 0.10, 28.3%) and South Asia (by 0.14, 31.1%). It also slightly increases AOD over regions influenced by wildfires, such as South America (by 0.02, 19.7%), Central Africa (by 0.03, 22.7%), and the boreal forests in Europe (by 0.01, 9.9%). Most increases occur near the surface (Figure B3), where the highest aerosol mass loading and mass extinction efficiency exist. The NRMSD between original and updated GEOS-Chem simulated AOD is 18.9% globally, and 25.6% over continents.

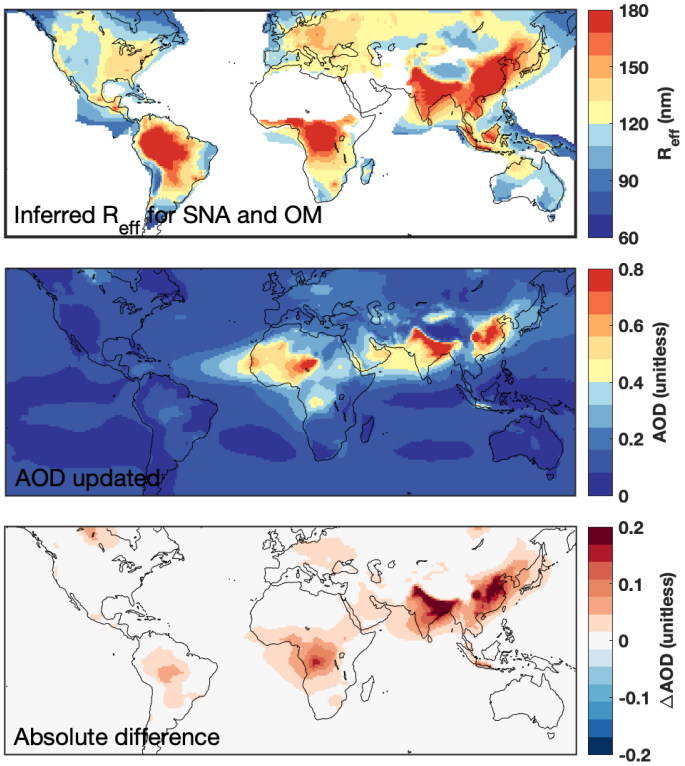

Figure 5. (Top) Surface dry R_{eff} for SNA and OM calculated using Eqn. (5) and GEOS-Chem bulk model simulated SNA and OM mass. R_{eff} is shown when M_{SNAOM} is greater than 80% of the total aerosol mass. (Middle) The GEOS-Chem simulated AOD using inferred R_{eff}. (Bottom) the absolute difference between updated AOD and default AOD using dry R_{eff} = 101 nm.

Although R_{eff} is only one of many processes affecting AOD, we evaluate the effect of the parameterization on the GEOS-Chem simulation of AOD to assess its implications. The left and middle panels of Figure 6 show the discrepancy between GEOS-Chem simulated AOD and AERONET AOD as a function of the parameterized surface R_{eff} for SNA and OM. The simulation using the default R_{eff} (Figure 6, left panel) slightly overestimates AOD at sites with small parameterized R_{eff} and underestimates AOD at sites with large parameterized R_{eff}. The overestimates occur primarily in western Europe where SNA and OM concentrations are low, while the underestimates happen mainly over industrial regions in East Asia, Southeast Asia, and biomass burning areas in South America and Central Africa,

where the SNA and OM mass loading are high (Figure B4). The underestimates are mitigated when applying the parameterized R_{eff} in GEOS-Chem (Figure 6, middle panel), yielding increased consistency between the measured (AERONET) AOD and simulated AOD (Figure 6, right; R^2 change from 0.68 to 0.74, slope from 0.75 to 0.94).

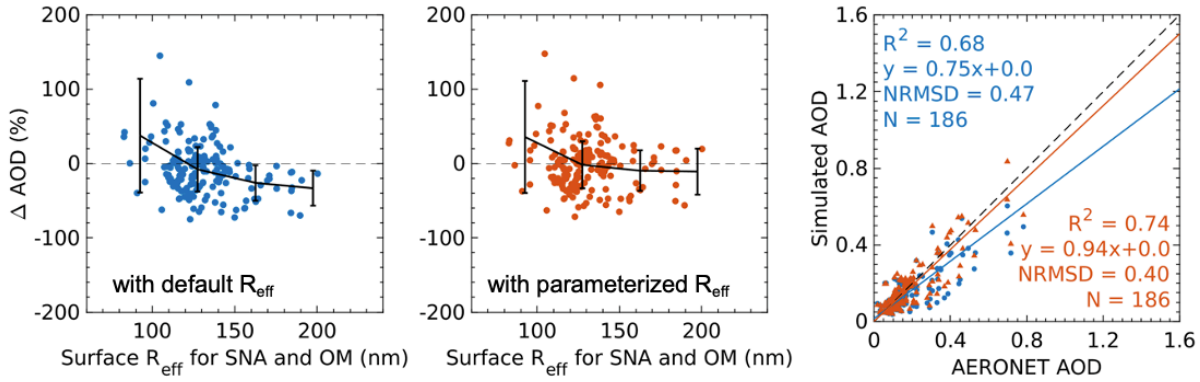

Figure 6. (Left and middle) Percent increase in GEOS-Chem simulated AOD minus AERONET AOD as a function of parameterized surface dry R_{eff} for SNA and OM. Black lines represent the mean values of ΔAOD in each 35 nm bin; error bars represent the corresponding standard deviation. (Right) Scatter plot of AERONET versus simulated AOD with the default R_{eff} (blue dots, line, and text), and with the parameterized R_{eff} (red dots, line, and text). The 1:1 line is dashed. NRMSD is the normalized root mean square deviation between the two datasets. N is the number of points in each dataset.

4 Conclusion

Aerosol size strongly determines mass scattering efficiency with implications for calculation of aerosol optical properties. Prior work found that the global mean dry aerosol size used in a bulk aerosol model induced low bias versus measured extinction in a region with a high aerosol loading (Zhai et al., 2021). We interpreted aircraft measurements from DISCOVER-AQ and KORUS-AQ with a chemical transport model (GEOS-Chem) to better understand regional variation in aerosol size. The measurements had a strong positive correlation (r = 0.83) between aerosol size and mass of sulfate-nitrate-ammonium (SNA) and organic matter (OM), reflecting the high condensation and coagulation rates where emissions of particles and the gaseous precursors are abundant, indicating the possibility of using aerosol mass as a predictor of aerosol size.

To gain a broader perspective of the global variation in aerosol size, we used the TOMAS microphysics package of the GEOS-Chem model to simulate the monthly mean aerosol mass, composition, and size distribution. We used effective radius (R_{eff}) as a surrogate of aerosol size and examined its relationship with aerosol mass and components where SNA and OM were dominant. We found that the sum of SNA and OM concentration, and the ratio between them, were the major predictors of R_{eff}. We used GEOS-Chem-TOMAS model output to derive a parameterization of R_{eff}, which well reproduced R_{eff} measured from the aircraft campaigns (R^2 = 0.74). When applied in the bulk GEOS-Chem high-performance model, the parameterization tended to increase R_{eff} of SNA and OM over regions with high concentrations of SNA and OM, and decrease R_{eff} elsewhere relative to the standard model. This led to a global

normalized root mean square deviation (NRMSD) of 43.8% between the original and updated surface R_{eff}. The parameterized R_{eff} tended to increase the vertical gradient in extinction relative to the standard model, due to the decrease in R_{eff} with altitude. The NRMSD of global mean AOD between the original and updated simulations was 18.9%, with the most significant regional AOD increase of 0.14 in South Asia, where aerosol mass loadings are high. This parameterization led to improved consistency of GEOS-Chem simulated AOD with AERONET AOD (R^2 from 0.68 to 0.74; slope from 0.75 to 0.94), by increasing AOD at high R_{eff}.

Overall, the simple parameterization of R_{eff} derived in this study improved the accuracy in modeling aerosol optical properties without imposing additional computational expense. Other chemical transport models and modeling of other size-related processes, such as heterogeneous chemistry, photolysis frequencies, and dry deposition, may also benefit from the parameterized R_{eff}. Future work could include additional parameters to better summarize the aerosol size distribution (Nair et al., 2021; Sakamoto et al., 2016). Further developments in computational efficiency of aerosol microphysics models and more abundant measurements of aerosol size and optical properties would both offer opportunities for further advances.

Data availability. AERONET data can be found at https://aeronet.gsfc.nasa.gov/. Aircraft data during DISCOVER-AQ are available at https://asdc.larc.nasa.gov/project/DISCOVER-AQ. KORUS-AQ data can be found at https://doi.org/10.5067/Suborbital/KORUSAQ/DATA01.

Author contributions. HZ and RVM designed the study. HZ performed the data analysis and model simulations with contributions from BC, SZ, CL, LB, JRP, IS, DC, and RYWC. BEA, LDZ, JWH, RAF, CAH, JLJ, PCJ, JED, JSS, AW, and BAN contributed to KORUS-AQ and DISCOVER-AQ campaign measurements. HZ and RVM wrote the paper with input from all authors.

Competing interests. The contact author has declared that neither they nor their co-authors have any competing interests.

Financial support. This work was supported by NASA Grant 80NSSC21K1343. JRP was funded by the US NSF Atmospheric Chemistry program, under grant AGS-1950327. JLJ and PCJ were supported by NASA Grant 80NSSC21K1451 and NNX15AT96G. BAN was supported by NASA Grant 80NSSC22K0283. JED was supported by NASA Grant NNX15AT88G.

Appendix A

A1 Application of spatially and temporally varying OM/OC ratio

The top panel of Figure A1 shows scatter plots of the estimated and measured OM/OC and OM during the KORUS-AQ campaign. The estimation is obtained by applying to OC measurement a NO_2 inferred OM/OC from (Philip et al., 2014), with a subsequent correction factor of 1.09 suggested by Canagaratna et al. (2015). Estimated OM is compared with measured OM by AMS during the campaign. Overall consistency is evident between NO_2-derived OM/OC and measured OM/OC. The agreement is better below 500 m than above (left panel, $R^2 = 0.62$ vs. 0.33). The discrepancy at high altitudes is mainly due to the low NO_2 (<0.2 ppbv), where the Philip *et al.* (2014) equation is not applicable. An average OM/OC ratio (2.1) is applied in this case. A high degree of consistency exists between the estimated OM and measured OM, with $R^2 = 0.99$ and slope = 0.91 for data from all altitudes (right panel), thus supporting the use of estimated OM in our analyses. The bottom left panel compares the vertical profile of the estimates and measurements, yielding overall consistency.

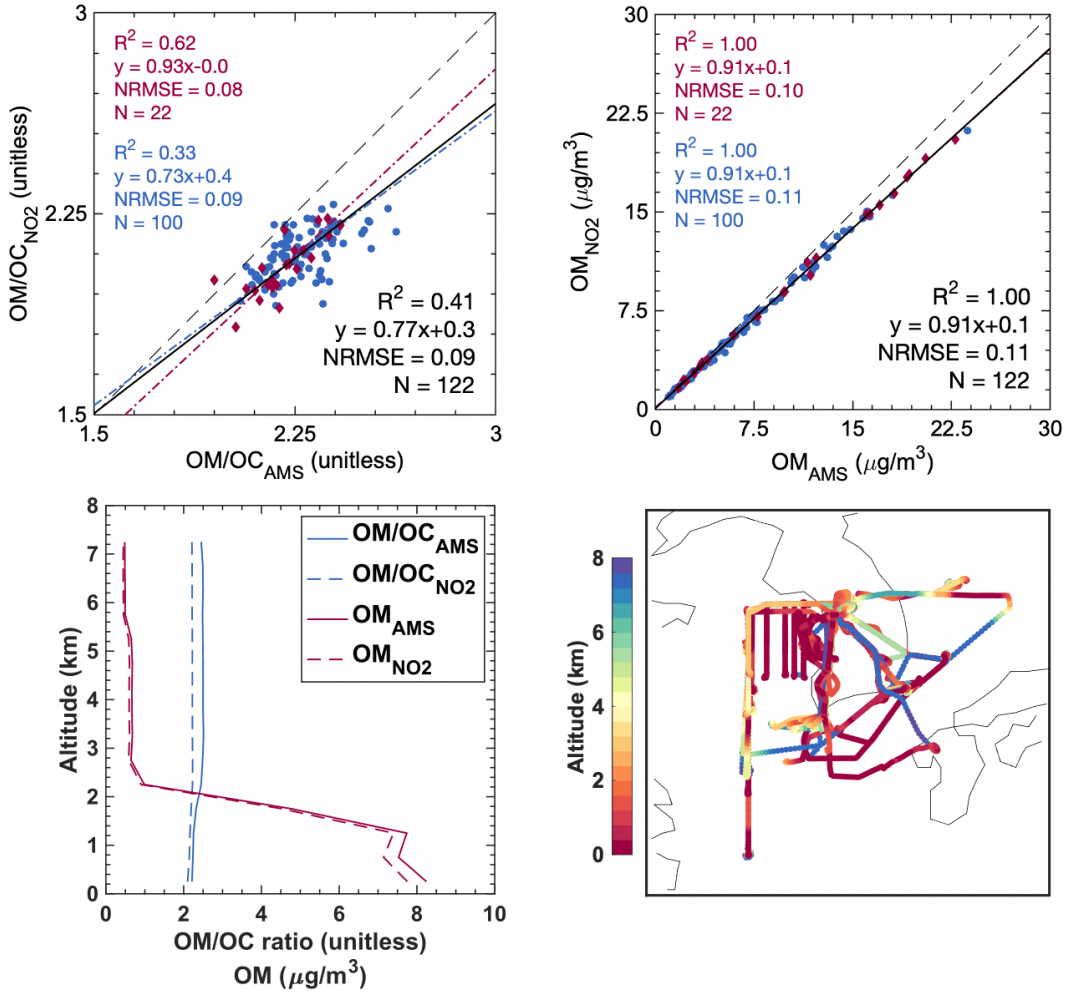

Figure A1. Scatter plots of estimated and measured OM/OC (top left) and OM (top right) during KORUS-AQ. Each point represents a mean value of AMS measurement for a 1-hour interval. Red diamonds, lines, and texts represent data from 0-500 m altitude. Blue dots, lines, and text represent data above 500 m from the ground. Black solid lines and texts represent the line of best fit for all the data. The 1:1 line is dashed. NRMSD is the normalized root mean square deviation between the two datasets. N is the number of points in each dataset. (Bottom left) Mean values of OM/OC and OM from measurements and estimations along the altitude. (Bottom right) Flight tracks during KORUS-AQ.

A2 Aerosol Extinction Calculation in GEOS-Chem

Extinction (Ext) of radiation by aerosols is represented as the sum of extinction due to each of the aerosol components using the following equation:

$$Ext_k = \frac{3Q_{ext,k}M_k}{4\rho_k R_{eff,k}} \quad \text{Eqn. (3)}$$

where subscript k indicates the property for the k^{th} component. R_{eff} is the effective radius defined as the area weighted mean radius. Q_{ext} is the area-weighted mean extinction efficiency. M is the aerosol mass loading per unit volume. ρ is the aerosol density. Aerosol optical depth (AOD) is the integral of aerosol extinction across the vertical domain.

For each component, extinction is calculated for assumed log-normal size distribution with corresponding dry geometric mean radius R_g and geometric standard deviation σ, hygroscopicity, refractive index (RI), and density (ρ) for individual aerosol components, as listed in Table A1. Sulfate, nitrate, and ammonium are grouped into SNA for convenience. R_{eff} and Q_{ext} are calculated using Mie Theory (Mishchenko et al., 1999, 2002) based on assumptions in aerosol size and RI. Hygroscopicity for SNA and OM is represented using a κ-Kohler hygroscopic growth scheme (Kreidenweis et al., 2008) as implemented by (Latimer and Martin, 2019).

Table A1. Dry aerosol properties in GEOS-Chem bulk model

Aerosol components	R_g, μm	σ	Hygroscopicity	Refractive Index (dry, 550 nm)	ρ, g cm^{-3}	R_{eff}, μm	Q_{ext}
SNA	0.058	1.6	$\kappa = 0.61$	$1.53 - 6.0\times10^{-3}i$	1.7	0.101	0.603
OM	0.058	1.6	$\kappa = 0.1$	$1.53 - 6.0\times10^{-3}i$	1.3	0.101	0.603

Appendix B

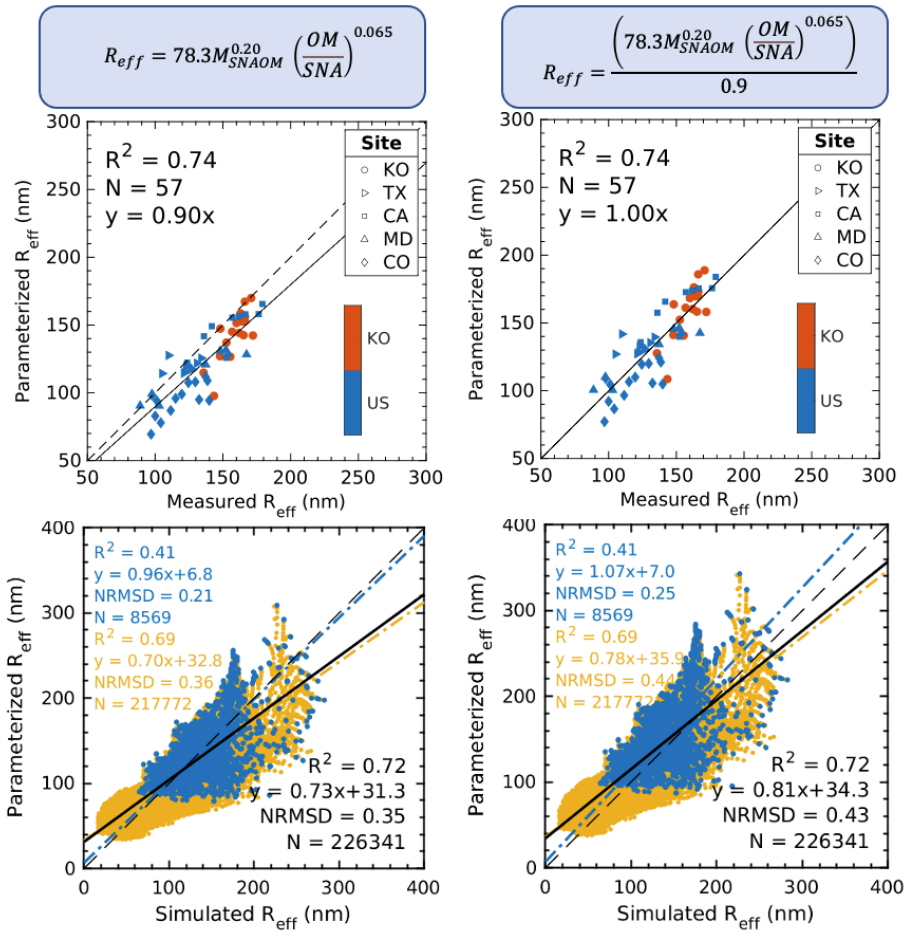

Figure B1. (Top) Scatter plot of parameterized R_{eff} and measured R_{eff} from DISCOVER-AQ and KORUS-AQ. Each point represents a daily mean measurement. (Bottom) Scatter plot of parameterized R_{eff} and GEOS-Chem-TOMAS simulated R_{eff} for the planetary boundary layer (blue dots, line, and texts), and for the free troposphere (yellow dots, line, and texts). Black solid lines and the texts indicate the entire troposphere with the sum of SNA and OM > 90% of aerosol mass. The 1:1 line is dashed. NRMSD is the normalized root mean square deviation between the two datasets. N is the number of points in each dataset. The left panel indicates the original parameterization from multiple linear regression. The right panel shows the adjusted parameterization using aircraft measurements.

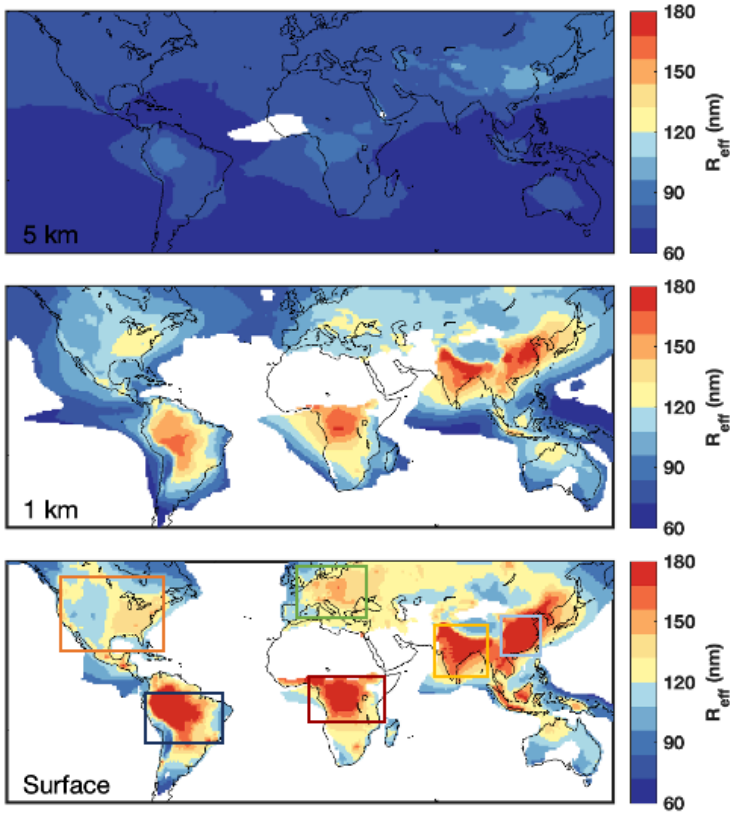

Figure B2. Annual mean R_{eff} for SNA and OM at (top) about 5 km, (middle) about 1 km, and (bottom) surface, calculated using Eqn. (5) and simulated SNA and OM mass from GEOS-Chem bulk model. R_{eff} is shown only if M_{SNAOM} is greater than 80% of the total aerosol mass. Boxes in the bottom panel define regions referred to in Figure B3.

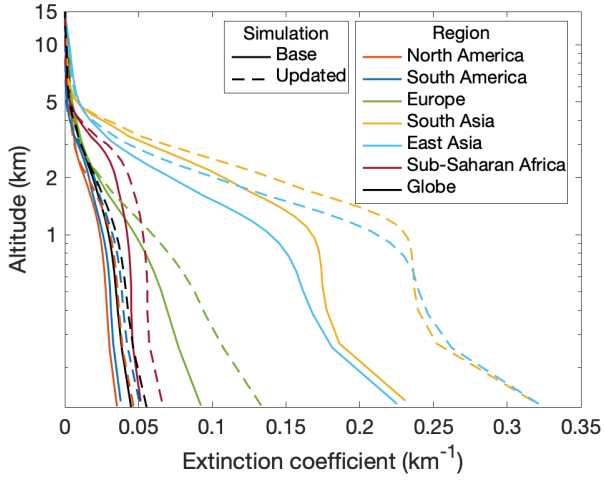

Figure B3. Global and regional aerosol extinction coefficient simulated by GEOS-Chem bulk model with original R_{eff} (solid lines) and parameterized R_{eff} (dashed lines). Regions are defined by the boxes in Figure B2.

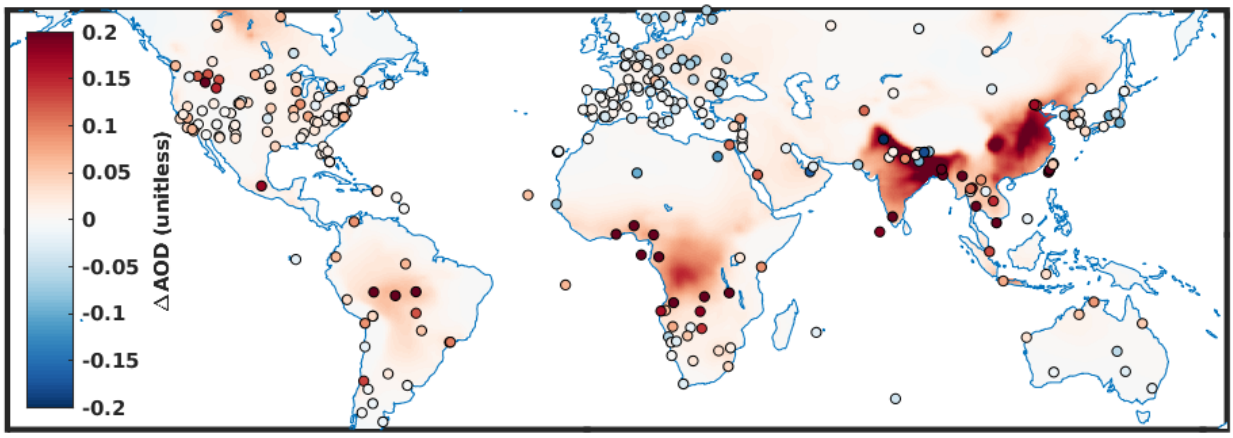

Figure B4. Difference between AERONET AOD minus default GEOS-Chem simulated AOD (dots) and difference between simulated AOD with the parameterized R_{eff} minus AOD with default R_{eff} (background).

Reference

Aalto, P., Hämeri, K., Becker, E. D. O., Weber, R., Salm, J., Mäkelä, J. M., Hoell, C., O'Dowd, C. D., Karlsson, H., Hansson, H., Väkevä, M., Koponen, I. K., Buzorius, G., and Kulmala, M.: Physical characterization of aerosol particles during nucleation events, Tellus B Chem Phys Meteorol, 53, 344–358, https://doi.org/10.3402/tellusb.v53i4.17127, 2001.

AboEl-Fetouh, Y., O'Neill, N. T., Kodros, J. K., Pierce, J. R., Lu, H., Ranjbar, K., and Xian, P.: Seasonal comparisons of GEOS-Chem-TOMAS (GCT) simulations with AERONET-inversion retrievals over sites in the North American and European Arctic, Atmos Environ, 271, 118852, https://doi.org/https://doi.org/10.1016/j.atmosenv.2021.118852, 2022.

Adams, P. J. and Seinfeld, J. H.: Predicting global aerosol size distributions in general circulation models, Journal of Geophysical Research Atmospheres, 107, AAC 4-1-AAC 4-23, https://doi.org/10.1029/2001JD001010, 2002.

Adams, P. J. and Seinfeld, J. H.: Disproportionate impact of particulate emissions on global cloud condensation nuclei concentrations, Geophys Res Lett, 30, 1–4, https://doi.org/10.1029/2002gl016303, 2003.

Andreae, M. O., Acevedo, O. C., Araùjo, A., Artaxo, P., Barbosa, C. G. G., Barbosa, H. M. J., Brito, J., Carbone, S., Chi, X., Cintra, B. B. L., Da Silva, N. F., Dias, N. L., Dias-Júnior, C. Q., Ditas, F., Ditz, R., Godoi, A. F. L., Godoi, R. H. M., Heimann, M., Hoffmann, T., Kesselmeier, J., Könemann, T., Krüger, M. L., Lavric, J. V., Manzi, A. O., Lopes, A. P., Martins, D. L., Mikhailov, E. F., Moran-Zuloaga, D., Nelson, B. W., Nölscher, A. C., Santos Nogueira, D., Piedade, M. T. F., Pöhlker, C., Pöschl, U., Quesada, C. A., Rizzo, L. V., Ro, C. U., Ruckteschler, N., Sá, L. D. A., De Oliveira Sá, M., Sales, C. B., Dos Santos, R. M. N., Saturno, J., Schöngart, J., Sörgel, M., De Souza, C. M., De Souza, R. A. F., Su, H., Targhetta, N., Tóta, J., Trebs, I., Trumbore, S., Van Eijck, A., Walter, D., Wang, Z., Weber, B., Williams, J., Winderlich, J., Wittmann, F., Wolff, S., and Yáñez-Serrano, A. M.: The Amazon Tall Tower Observatory (ATTO): Overview of pilot measurements on ecosystem ecology, meteorology, trace gases, and aerosols, Atmos Chem Phys, 15, 10723–10776, https://doi.org/10.5194/acp-15-10723-2015, 2015.

Asmi, A., Wiedensohler, A., Laj, P., Fjaeraa, A. M., Sellegri, K., Birmili, W., Weingartner, E., Baltensperger, U., Zdimal, V., Zikova, N., Putaud, J. P., Marinoni, A., Tunved, P., Hansson, H. C., Fiebig, M., Kivekäs, N., Lihavainen, H., Asmi, E., Ulevicius, V., Aalto, P. P., Swietlicki, E., Kristensson, A., Mihalopoulos, N., Kalivitis, N., Kalapov, I., Kiss, G., de Leeuw, G., Henzing, B., Harrison, R. M., Beddows, D., O'Dowd, C., Jennings, S. G., Flentje, H., Weinhold, K., Meinhardt, F., Ries, L., and Kulmala, M.: Number size distributions and seasonality of submicron particles in Europe 2008-2009, Atmos Chem Phys, 11, 5505–5538, https://doi.org/10.5194/acp-11-5505-2011, 2011.

Bahreini, R., Jimenez, J. L., Wang, J., Flagan, R. C., Seinfeld, J. H., Jayne, J. T., and Worsnop, D. R.: Aircraft-based aerosol size and composition measurements during ACE-Asia using an Aerodyne aerosol mass spectrometer, Journal of Geophysical Research: Atmospheres, 108, https://doi.org/10.1029/2002jd003226, 2003.

Bindle, L., Martin, R. V., Cooper, M. J., Lundgren, E. W., Eastham, S. D., Auer, B. M., Clune, T. L., Weng, H., Lin, J., Murray, L. T., Meng, J., Keller, C. A., Putman, W. M., Pawson, S., and Jacob, D. J.: Grid-stretching capability for

the GEOS-Chem 13.0.0 atmospheric chemistry model, Geosci Model Dev, 14, 5977–5997, https://doi.org/10.5194/gmd-14-5977-2021, 2021.

Canagaratna, M. R., Jayne, J. T., Jimenez, J. L., Allan, J. D., Alfarra, M. R., Zhang, Q., Onasch, T. B., Drewnick, F., Coe, H., and Middlebrook, A.: Chemical and microphysical characterization of ambient aerosols with the aerodyne aerosol mass spectrometer, Mass Spectrom Rev, 26, 185–222, https://doi.org/doi:10.1002/mas.20115, 2007.

Canagaratna, M. R., Jimenez, J. L., Kroll, J. H., Chen, Q., Kessler, S. H., Massoli, P., Hildebrandt Ruiz, L., Fortner, E., Williams, L. R., Wilson, K. R., Surratt, J. D., Donahue, N. M., Jayne, J. T., and Worsnop, D. R.: Elemental ratio measurements of organic compounds using aerosol mass spectrometry: Characterization, improved calibration, and implications, Atmos Chem Phys, 15, 253–272, https://doi.org/10.5194/acp-15-253-2015, 2015.

Choi, S., Lamsal, L. N., Follette-Cook, M., Joiner, J., Krotkov, N. A., Swartz, W. H., Pickering, K. E., Loughner, C. P., Appel, W., Pfister, G., Saide, P. E., Cohen, R. C., Weinheimer, A. J., and Herman, J. R.: Assessment of NO2 observations during DISCOVER-AQ and KORUS-AQ field campaigns, Atmos Meas Tech, 13, 2523–2546, https://doi.org/10.5194/amt-13-2523-2020, 2020.

Chu, D. A., Ferrare, R., Szykman, J., Lewis, J., Scarino, A., Hains, J., Burton, S., Chen, G., Tsai, T., Hostetler, C., Hair, J., Holben, B., and Crawford, J.: Regional characteristics of the relationship between columnar AOD and surface PM2.5: Application of lidar aerosol extinction profiles over Baltimore-Washington Corridor during DISCOVER-AQ, Atmos Environ, 101, 338e349-349, https://doi.org/10.1016/j.atmosenv.2014.11.034, 2015.

Croft, B., Lohmann, U., and von Salzen, K.: Black carbon ageing in the Canadian Centre for Climate modelling and analysis atmospheric general circulation model, Atmos Chem Phys, 5, 1931–1949, https://doi.org/10.5194/acp-5-1931-2005, 2005.

D'Andrea, S. D., Häkkinen, S. A. K., Westervelt, D. M., Kuang, C., Levin, E. J. T., Kanawade, V. P., Leaitch, W. R., Spracklen, D. V., Riipinen, I., and Pierce, J. R.: Understanding global secondary organic aerosol amount and size-resolved condensational behavior, Atmos Chem Phys, 13, 11519–11534, https://doi.org/10.5194/acp-13-11519-2013, 2013.

Dibb, J. E., Talbot, R. W., Scheuer, E. M., Seid, G., Avery, M. A., and Singh, H. B.: Aerosol chemical composition in Asian continental outflow during the TRACE-P campaign: Comparison with PEM-West B, Journal of Geophysical Research: Atmospheres, 108, https://doi.org/10.1029/2002jd003111, 2003.

Van Donkelaar, A., Martin, R. V., Li, C., and Burnett, R. T.: Regional Estimates of Chemical Composition of Fine Particulate Matter Using a Combined Geoscience-Statistical Method with Information from Satellites, Models, and Monitors, Environ Sci Technol, 53, 2595–2611, https://doi.org/10.1021/acs.est.8b06392, 2019.

Eastham, S. D., Long, M. S., Keller, C. A., Lundgren, E., Yantosca, R. M., Zhuang, J., Li, C., Lee, C. J., Yannetti, M., Auer, B. M., Clune, T. L., Kouatchou, J., Putman, W. M., Thompson, M. A., Trayanov, A. L., Molod, A. M., Martin, R. V., and Jacob, D. J.: GEOS-Chem high performance (GCHP v11-02c): A next-generation implementation of the

GEOS-Chem chemical transport model for massively parallel applications, Geosci Model Dev, 11, 2941–2953, https://doi.org/10.5194/gmd-11-2941-2018, 2018.

Emerson, E. W., Hodshire, A. L., DeBolt, H. M., Bilsback, K. R., Pierce, J. R., McMeeking, G. R., and Farmer, D. K.: Revisiting particle dry deposition and its role in radiative effect estimates, Proc Natl Acad Sci U S A, 117, 26076–26082, https://doi.org/10.1073/pnas.2014761117, 2020.

Ervens, B., Turpin, B. J., and Weber, R. J.: Secondary organic aerosol formation in cloud droplets and aqueous particles (aqSOA): A review of laboratory, field and model studies, Atmos Chem Phys, 11, 11069–11102, https://doi.org/10.5194/acp-11-11069-2011, 2011.

Estillore, A. D., Trueblood, J. V., and Grassian, V. H.: Atmospheric chemistry of bioaerosols: Heterogeneous and multiphase reactions with atmospheric oxidants and other trace gases, Chem Sci, 7, 6604–6616, https://doi.org/10.1039/c6sc02353c, 2016.

Fairlie, D. T., Jacob, D. J., and Park, R. J.: The impact of transpacific transport of mineral dust in the United States, Atmos Environ, 41, 1251–1266, https://doi.org/10.1016/j.atmosenv.2006.09.048, 2007.

Faxvog, F. R. and Roessler, D. M.: Carbon aerosol visibility vs particle size distribution, Appl Opt, 17, 2612, https://doi.org/10.1364/ao.17.002612, 1978.

Fountoukis, C. and Nenes, A.: ISORROPIAII: A computationally efficient thermodynamic equilibrium model for K+-Ca2+-Mg2+-NH4+-Na+-SO42--NO3--Cl--H2O aerosols, Atmos Chem Phys, 7, 4639–4659, https://doi.org/10.5194/acp-7-4639-2007, 2007.

GCST, Yu, F., and Luo, G.: APM aerosol microphysics, http://wiki.seas.harvard.edu/geos-chem/index.php/APM_aerosol_microphysics, last access: 23 January, 2023.

Geng, G., Zhang, Q., Tong, D., Li, M., Zheng, Y., Wang, S., and He, K.: Chemical composition of ambient PM2. 5 over China and relationship to precursor emissions during 2005-2012, Atmos Chem Phys, 17, 9187–9203, https://doi.org/10.5194/acp-17-9187-2017, 2017.

Giles, D. M., Sinyuk, A., Sorokin, M. G., Schafer, J. S., Smirnov, A., Slutsker, I., Eck, T. F., Holben, B. N., Lewis, J. R., Campbell, J. R., Welton, E. J., Korkin, S. V., and Lyapustin, A. I.: Advancements in the Aerosol Robotic Network (AERONET) Version 3 database - Automated near-real-time quality control algorithm with improved cloud screening for Sun photometer aerosol optical depth (AOD) measurements, Atmos Meas Tech, 12, 169–209, https://doi.org/10.5194/amt-12-169-2019, 2019.

Guo, H., Campuzano-Jost, P., Nault, B. A., Day, D. A., Schroder, J. C., Kim, D., Dibb, J. E., Dollner, M., Weinzierl, B., and Jimenez, J. L.: The importance of size ranges in aerosol instrument intercomparisons: A case study for the Atmospheric Tomography Mission, Atmos Meas Tech, 14, 3631–3655, https://doi.org/10.5194/amt-14-3631-2021, 2021.

573 Hair, J. W., Hostetler, C. A., Cook, A. L., Harper, D. B., Ferrare, R. A., Mack, T. L., Welch, W., Izquierdo, L. R., and
574 Hovis, F. E.: Airborne High Spectral Resolution Lidar for profiling Aerosol optical properties, Appl Opt, 47, 6734–
575 6753, https://doi.org/10.1364/AO.47.006734, 2008.

576 Hammer, M. S., Martin, R. V., Van Donkelaar, A., Buchard, V., Torres, O., Ridley, D. A., and Spurr, R. J. D.:
577 Interpreting the ultraviolet aerosol index observed with the OMI satellite instrument to understand absorption by
578 organic aerosols: Implications for atmospheric oxidation and direct radiative effects, Atmos Chem Phys, 16, 2507–
579 2523, https://doi.org/10.5194/acp-16-2507-2016, 2016.

580 Hansen, J. E. and Travis, L. D.: Light scattering in planetary atmospheres, Space Sci Rev, 16, 527–610,
581 https://doi.org/10.1007/BF00168069, 1974.

582 Hayes, P. L., Ortega, A. M., Cubison, M. J., Froyd, K. D., Zhao, Y., Cliff, S. S., Hu, W. W., Toohey, D. W., Flynn, J.
583 H., Lefer, B. L., Grossberg, N., Alvarez, S., Rappenglück, B., Taylor, J. W., Allan, J. D., Holloway, J. S., Gilman, J.
584 B., Kuster, W. C., De Gouw, J. A., Massoli, P., Zhang, X., Liu, J., Weber, R. J., Corrigan, A. L., Russell, L. M.,
585 Isaacman, G., Worton, D. R., Kreisberg, N. M., Goldstein, A. H., Thalman, R., Waxman, E. M., Volkamer, R., Lin,
586 Y. H., Surratt, J. D., Kleindienst, T. E., Offenberg, J. H., Dusanter, S., Griffith, S., Stevens, P. S., Brioude, J., Angevine,
587 W. M., and Jimenez, J. L.: Organic aerosol composition and sources in Pasadena, California, during the 2010 CalNex
588 campaign, Journal of Geophysical Research Atmospheres, 118, 9233–9257, https://doi.org/10.1002/jgrd.50530, 2013.

589 Hinds, W. C. and Zhu, Y.: Aerosol technology: Properties, behavior, and measurement of airborne particles, Second.,
590 Wiley, New York, 1999.

591 Huang, Y., Li, L., Li, J., Wang, X., Chen, H., Chen, J., Yang, X., Gross, D. S., Wang, H., Qiao, L., and Chen, C.: A
592 case study of the highly time-resolved evolution of aerosol chemical and optical properties in urban Shanghai, China,
593 Atmos Chem Phys, 13, 3931–3944, https://doi.org/10.5194/acp-13-3931-2013, 2013.

594 Jaeglé, L., Quinn, P. K., Bates, T. S., Alexander, B., and Lin, J. T.: Global distribution of sea salt aerosols: New
595 constraints from in situ and remote sensing observations, Atmos Chem Phys, 11, 3137–3157,
596 https://doi.org/10.5194/acp-11-3137-2011, 2011.

597 Janẗall, S., Andreae, M. O., and Pöschl, U.: Biomass burning aerosol emissions from vegetation fires: Particle number
598 and mass emission factors and size distributions, Atmos Chem Phys, 10, 1427–1439, https://doi.org/10.5194/acp-10-
599 1427-2010, 2010.

600 Jin, J., Henzing, B., and Segers, A.: How aerosol size matters in aerosol optical depth (AOD) assimilation and the
601 optimization using the Ångström exponent, Atmos Chem Phys, 23, 1641–1660, https://doi.org/10.5194/acp-23-1641-
602 2023, 2023.

603 Jordan, C. E., Crawford, J. H., Beyersdorf, A. J., Eck, T. F., Halliday, H. S., Nault, B. A., Chang, L.-S., Park, J., Park,
604 R., and Lee, G.: Investigation of factors controlling PM2. 5 variability across the South Korean Peninsula during
605 KORUS-AQ, Elementa: Science of the Anthropocene, 8, 2020.

606 Kahn, R. A., Gaitley, B. J., Martonchik, J. v., Diner, D. J., Crean, K. A., and Holben, B.: Multiangle Imaging
607 Spectroradiometer (MISR) global aerosol optical depth validation based on 2 years of coincident Aerosol Robotic
608 Network (AERONET) observations, Journal of Geophysical Research D: Atmospheres, 110, 1–16,
609 https://doi.org/10.1029/2004JD004706, 2005.

610 Karydis, V. A., Kumar, P., Barahona, D., Sokolik, I. N., and Nenes, A.: On the effect of dust particles on global cloud
611 condensation nuclei and cloud droplet number, Journal of Geophysical Research Atmospheres, 116,
612 https://doi.org/10.1029/2011JD016283, 2011.

613 Kellogg, W. W.: Aerosols and Climate., Science (1979), 183, 281–296,
614 https://doi.org/10.1093/oso/9780198779308.003.0005, 1980.

615 Kodros, J. K. and Pierce, J. R.: Important global and regional differences in aerosol cloud-albedo effect estimates
616 between simulations with and without prognostic aerosol microphysics, J Geophys Res, 122, 4003–4018,
617 https://doi.org/10.1002/2016JD025886, 2017.

618 Kodros, J. K., Volckens, J., Jathar, S. H., and Pierce, J. R.: Ambient particulate matter size distributions drive regional
619 and global variability in particle deposition in the respiratory tract, Geohealth, 2, 298–312,
620 https://doi.org/10.1029/2018gh000145, 2018.

621 Koffi, B., Schulz, M., Bréon, F. M., Dentener, F., Steensen, B. M., Griesfeller, J., Winker, D., Balkanski, Y., Bauer,
622 S. E., Bellouin, N., Berntsen, T., Bian, H., Chin, M., Diehl, T., Easter, R., Ghan, S., Hauglustaine, D. A., Iversen, T.,
623 Kirkevåg, A., Liu, X., Lohmann, U., Myhre, G., Rasch, P., Seland, Ø., Skeie, R. B., Steenrod, S. D., Stier, P., Tackett,
624 J., Takemura, T., Tsigaridis, K., Vuolo, M. R., Yoon, J., and Zhang, K.: Evaluation of the aerosol vertical distribution
625 in global aerosol models through comparison against CALIOP measurements: AeroCom phase II results, J Geophys
626 Res, 121, 7254–7283, https://doi.org/10.1002/2015JD024639, 2016.

627 Kopke P., H. M. S. I. S. E. P.: Aerosol data set, Max Planck Institut fur Meteorologie, Report No. 243, Hamburg,
628 https://doi.org/Report No. 243, 1997.

629 Kreidenweis, S. M., Petters, M. D., and DeMott, P. J.: Single-parameter estimates of aerosol water content,
630 Environmental Research Letters, 3, 35002, 2008.

631 Lamarque, J. F., Shindell, D. T., Josse, B., Young, P. J., Cionni, I., Eyring, V., Bergmann, D., Cameron-Smith, P.,
632 Collins, W. J., Doherty, R., Dalsoren, S., Faluvegi, G., Folberth, G., Ghan, S. J., Horowitz, L. W., Lee, Y. H.,
633 MacKenzie, I. A., Nagashima, T., Naik, V., Plummer, D., Righi, M., Rumbold, S. T., Schulz, M., Skeie, R. B.,
634 Stevenson, D. S., Strode, S., Sudo, K., Szopa, S., Voulgarakis, A., and Zeng, G.: The atmospheric chemistry and
635 climate model intercomparison Project (ACCMIP): Overview and description of models, simulations and climate
636 diagnostics, Geosci Model Dev, 6, 179–206, https://doi.org/10.5194/gmd-6-179-2013, 2013.

637 Lamb, K. D., Perring, A. E., Samset, B., Peterson, D., Davis, S., Anderson, B. E., Beyersdorf, A., Blake, D. R.,
638 Campuzano-Jost, P., Corr, C. A., Diskin, G. S., Kondo, Y., Moteki, N., Nault, B. A., Oh, J., Park, M., Pusede, S. E.,
639 Simpson, I. J., Thornhill, K. L., Wisthaler, A., and Schwarz, J. P.: Estimating Source Region Influences on Black

Carbon Abundance, Microphysics, and Radiative Effect Observed Over South Korea, Journal of Geophysical Research: Atmospheres, 123, 13,527-13,548, https://doi.org/10.1029/2018JD029257, 2018.

Latimer, R. N. C. and Martin, R. v.: Interpretation of measured aerosol mass scattering efficiency over North America using a chemical transport model, Atmos Chem Phys, 19, 2635–2653, https://doi.org/10.5194/acp-19-2635-2019, 2019.

Lee, Y. N., Weber, R., Ma, Y., Orsini, D., Maxwell-Meier, K., Blake, D., Meinardi, S., Sachse, G., Harward, C., Chen, T. Y., Thornton, D., Tu, F. H., and Bandy, A.: Airborne measurement of inorganic ionic components of fine aerosol particles using the particle-into-liquid sampler coupled to ion chromatography technique during ACE-Asia and TRACE-P, Journal of Geophysical Research: Atmospheres, 108, https://doi.org/10.1029/2002jd003265, 2003.

Levy, R. C., Mattoo, S., Munchak, L. A., Remer, L. A., Sayer, A. M., Patadia, F., and Hsu, N. C.: The Collection 6 MODIS aerosol products over land and ocean, Atmos Meas Tech, 6, 2989–3034, https://doi.org/10.5194/amt-6-2989-2013, 2013.

Li, C., Martin, R. V, van Donkelaar, A., Boys, B. L., Hammer, M. S., Xu, J.-W., Marais, E. A., Reff, A., Strum, M., and Ridley, D. A.: Trends in chemical composition of global and regional population-weighted fine particulate matter estimated for 25 years, Environ Sci Technol, 51, 11185–11195, 2017.

Liu, H., Jacob, D. J., Bey, I., and Yantosca, R. M.: Constraints from 210Pb and 7Be on wet deposition and transport in a global three-dimensional chemical tracer model driven by assimilated meteorological fields, Journal of Geophysical Research Atmospheres, 106, 12109–12128, https://doi.org/10.1029/2000JD900839, 2001.

Liu, X., Easter, R. C., Ghan, S. J., Zaveri, R., Rasch, P., Shi, X., Lamarque, J. F., Gettelman, A., Morrison, H., Vitt, F., Conley, A., Park, S., Neale, R., Hannay, C., Ekman, A. M. L., Hess, P., Mahowald, N., Collins, W., Iacono, M. J., Bretherton, C. S., Flanner, M. G., and Mitchell, D.: Toward a minimal representation of aerosols in climate models: Description and evaluation in the Community Atmosphere Model CAM5, Geosci Model Dev, 5, 709–739, https://doi.org/10.5194/gmd-5-709-2012, 2012.

Liu, X., Ma, P.-L., Wang, H., Tilmes, S., Singh, B., Easter, R. C., Ghan, S. J., and Rasch, P. J.: Description and evaluation of a new four-mode version of the Modal Aerosol Module (MAM4) within version 5.3 of the Community Atmosphere Model, Geosci Model Dev, 9, 505–522, 2016.

Lyapustin, A., Wang, Y., Korkin, S., and Huang, D.: MODIS Collection 6 MAIAC algorithm, Atmos Meas Tech, 11, 5741–5765, https://doi.org/10.5194/amt-11-5741-2018, 2018.

Malm, W. C., Sisler, J. F., Huffman, D., Eldred, R. A., and Cahill, T. A.: Spatial and seasonal trends in particle concentration and optical extinction in the United States, J Geophys Res, 99, 1347–1370, https://doi.org/10.1029/93JD02916, 1994.

Mann, G. W., Carslaw, K. S., Spracklen, D. V., Ridley, D. A., Manktelow, P. T., Chipperfield, M. P., Pickering, S. J., and Johnson, C. E.: Description and evaluation of GLOMAP-mode: A modal global aerosol microphysics model for

673 the UKCA composition-climate model, Geosci Model Dev, 3, 519–551, https://doi.org/10.5194/gmd-3-519-2010,
674 2010.

675 Marais, E. A., Jacob, D. J., Jimenez, J. L., Campuzano-Jost, P., Day, D. A., Hu, W., Krechmer, J., Zhu, L., Kim, P. S.,
676 Miller, C. C., Fisher, J. A., Travis, K., Yu, K., Hanisco, T. F., Wolfe, G. M., Arkinson, H. L., Pye, H. O. T., Froyd, K.
677 D., Liao, J., and McNeill, V. F.: Aqueous-phase mechanism for secondary organic aerosol formation from isoprene:
678 Application to the southeast United States and co-benefit of SO2 emission controls, Atmos Chem Phys, 16, 1603–
679 1618, https://doi.org/10.5194/acp-16-1603-2016, 2016.

680 Martin, R. V., Jacob, D. J., Yantosca, R. M., Chin, M., and Ginoux, P.: Global and regional decreases in tropospheric
681 oxidants from photochemical effects of aerosols, Journal of Geophysical Research: Atmospheres, 108,
682 https://doi.org/10.1029/2002jd002622, 2003.

683 Martin, R. V, Eastham, S. D., Bindle, L., Lundgren, E. W., Clune, T. L., Keller, C. A., Downs, W., Zhang, D., Lucchesi,
684 R. A., Sulprizio, M. P., Yantosca, R. M., Li, Y., Estrada, L., Putman, W. M., Auer, B. M., Trayanov, L., Pawson, S.,
685 and Jacob, D. J.: Improved Advection , Resolution , Performance , and Community Access in the New Generation
686 (Version 13) of the High Performance GEOS-Chem Global Atmospheric Chemistry Model (GCHP), Geoscientific
687 Model Development Discussions, 720, 1–30, https://doi.org/10.5194/gmd-2022-42, 2022.

688 McDuffie, E. E., Smith, S. J., O'Rourke, P., Tibrewal, K., Venkataraman, C., Marais, E. A., Zheng, B., Crippa, M.,
689 Brauer, M., and Martin, R. V.: A global anthropogenic emission inventory of atmospheric pollutants from sector- And
690 fuel-specific sources (1970-2017): An application of the Community Emissions Data System (CEDS), Earth Syst Sci
691 Data, 12, 3413–3442, https://doi.org/10.5194/essd-12-3413-2020, 2020.

692 McDuffie, E. E., Martin, R. V., Spadaro, J. V., Burnett, R., Smith, S. J., O'Rourke, P., Hammer, M. S., van Donkelaar,
693 A., Bindle, L., Shah, V., Jaeglé, L., Luo, G., Yu, F., Adeniran, J. A., Lin, J., and Brauer, M.: Source sector and fuel
694 contributions to ambient PM2.5 and attributable mortality across multiple spatial scales, Nat Commun, 12, 1–12,
695 https://doi.org/10.1038/s41467-021-23853-y, 2021.

696 McNaughton, C. S., Clarke, A. D., Howell, S. G., Pinkerton, M., Anderson, B., Thornhill, L., Hudgins, C., Winstead,
697 E., Dibb, J. E., Scheuer, E., and Maring, H.: Results from the DC-8 inlet characterization experiment (DICE): Airborne
698 versus surface sampling of mineral dust and sea salt aerosols, Aerosol Science and Technology, 41, 136–159,
699 https://doi.org/10.1080/02786820601118406, 2007.

700 Meng, J., Martin, R. V., Li, C., Van Donkelaar, A., Tzompa-Sosa, Z. A., Yue, X., Xu, J. W., Weagle, C. L., and
701 Burnett, R. T.: Source Contributions to Ambient Fine Particulate Matter for Canada, Environ Sci Technol, 53, 10269–
702 10278, https://doi.org/10.1021/acs.est.9b02461, 2019.

703 Meng, J., Martin, R. v., Ginoux, P., Hammer, M., Sulprizio, M. P., Ridley, D. A., and van Donkelaar, A.: Grid-
704 independent high-resolution dust emissions (v1.0) for chemical transport models: Application to GEOS-Chem (12.5.0),
705 Geosci Model Dev, 14, 4249–4260, https://doi.org/10.5194/gmd-14-4249-2021, 2021a.

706 Meng, J., Martin, R. V., Ginoux, P., Hammer, M., Sulprizio, M. P., Ridley, D. A., and Van Donkelaar, A.: Grid-
707 independent high-resolution dust emissions (v1.0) for chemical transport models: Application to GEOS-Chem (12.5.0),
708 Geosci Model Dev, 14, 4249–4260, https://doi.org/10.5194/gmd-14-4249-2021, 2021b.

709 Mishchenko, M. I., Dlugach, J. M., Yanovitskij, E. G., and Zakharova, N. T.: Bidirectional reflectance of flat, optically
710 thick particulate layers: An efficient radiative transfer solution and applications to snow and soil surfaces, J Quant
711 Spectrosc Radiat Transf, 63, 409–432, https://doi.org/10.1016/S0022-4073(99)00028-X, 1999.

712 Mishchenko, M. I., Travis, L. D., and Lacis, A. a: Scattering, Absorption, and Emission of Light by Small Particles,
713 Cambridge University Press, Cambridge, 1–486 pp., 2002.

714 Moore, R. H., Wiggins, E. B., Ahern, A. T., Zimmerman, S., Montgomery, L., Campuzano Jost, P., Robinson, C. E.,
715 Ziemba, L. D., Winstead, E. L., Anderson, B. E., Brock, C. A., Brown, M. D., Chen, G., Crosbie, E. C., Guo, H.,
716 Jimenez, J. L., Jordan, C. E., Lyu, M., Nault, B. A., Rothfuss, N. E., Sanchez, K. J., Schueneman, M., Shingler, T. J.,
717 Shook, M. A., Thornhill, K. L., Wagner, N. L., and Wang, J.: Sizing response of the Ultra-High Sensitivity Aerosol
718 Spectrometer (UHSAS) and Laser Aerosol Spectrometer (LAS) to changes in submicron aerosol composition and
719 refractive index, Atmos Meas Tech, 14, 4517–4542, https://doi.org/10.5194/amt-14-4517-2021, 2021.

720 Nair, A. A., Yu, F., Campuzano-Jost, P., DeMott, P. J., Levin, E. J. T., Jimenez, J. L., Peischl, J., Pollack, I. B.,
721 Fredrickson, C. D., and Beyersdorf, A. J.: Machine learning uncovers aerosol size information from chemistry and
722 meteorology to quantify potential cloud-forming particles, Geophys Res Lett, 48, e2021GL094133, 2021.

723 Napari, I., Noppel, M., Vehkamäki, H., and Kulmala, M.: Parametrization of ternary nucleation rates for H2so4-NH3-
724 H2O vapors, Journal of Geophysical Research Atmospheres, 107, AAC 6-1-AAC 6-6,
725 https://doi.org/10.1029/2002JD002132, 2002.

726 Nault, B. A., Campuzano-Jost, P., Day, D. A., Schroder, J. C., Anderson, B., Beyersdorf, A. J., Blake, D. R., Brune,
727 W. H., Choi, Y., Corr, C. A., de Gouw, J. A., Dibb, J., Digangi, J. P., Diskin, G. S., Fried, A., Gregory Huey, L., Kim,
728 M. J., Knote, C. J., Lamb, K. D., Lee, T., Park, T., Pusede, S. E., Scheuer, E., Thornhill, K. L., Woo, J. H., and Jimenez,
729 J. L.: Secondary organic aerosol production from local emissions dominates the organic aerosol budget over Seoul,
730 South Korea, during KORUS-AQ, Atmos Chem Phys, 18, 17769–17800, https://doi.org/10.5194/acp-18-17769-2018,
731 2018.

732 Ngo, N. S., Asseko, S. V. J., Ebanega, M. O., Allo'o Allo'o, S. M., and Hystad, P.: The relationship among PM2.5,
733 traffic emissions, and socioeconomic status: Evidence from Gabon using low-cost, portable air quality monitors,
734 Transp Res D Transp Environ, 68, 2–9, https://doi.org/10.1016/j.trd.2018.01.029, 2019.

735 Park, R. J.: Natural and transboundary pollution influences on sulfate-nitrate-ammonium aerosols in the United States:
736 Implications for policy, J Geophys Res, 109, https://doi.org/10.1029/2003jd004473, 2004.

737 Park, R. J., Jacob, D. J., Chin, M., and Martin, R. V.: Sources of carbonaceous aerosols over the United States and
738 implications for natural visibility, Journal of Geophysical Research Atmospheres, 108,
739 https://doi.org/10.1029/2002jd003190, 2003.

740 Park, S.-S., Sim, S. Y., Bae, M.-S., and Schauer, J. J.: Size distribution of water-soluble components in particulate
741 matter emitted from biomass burning, Atmos Environ, 73, 62–72, 2013.

742 Philip, S., Martin, R. V., Pierce, J. R., Jimenez, J. L., Zhang, Q., Canagaratna, M. R., Spracklen, D. V., Nowlan, C.
743 R., Lamsal, L. N., Cooper, M. J., and Krotkov, N. A.: Spatially and seasonally resolved estimate of the ratio of organic
744 mass to organic carbon, Atmos Environ, 87, 34–40, https://doi.org/10.1016/j.atmosenv.2013.11.065, 2014.

745 Philip, S., Martin, R. V., Snider, G., Weagle, C. L., Van Donkelaar, A., Brauer, M., Henze, D. K., Klimont, Z.,
746 Venkataraman, C., Guttikunda, S. K., and Zhang, Q.: Anthropogenic fugitive, combustion and industrial dust is a
747 significant, underrepresented fine particulate matter source in global atmospheric models, Environmental Research
748 Letters, 12, https://doi.org/10.1088/1748-9326/aa65a4, 2017.

749 Pierce, J. R., Chen, K., and Adams, P. J.: Contribution of primary carbonaceous aerosol to cloud condensation nuclei:
750 Processes and uncertainties evaluated with a global aerosol microphysics model, Atmos Chem Phys, 7, 5447–5466,
751 https://doi.org/10.5194/acp-7-5447-2007, 2007.

752 Pierce, J. R., Croft, B., Kodros, J. K., D'Andrea, S. D., and Martin, R. V.: The importance of interstitial particle
753 scavenging by cloud droplets in shaping the remote aerosol size distribution and global aerosol-climate effects, Atmos
754 Chem Phys, 15, 6147–6158, https://doi.org/10.5194/acp-15-6147-2015, 2015.

755 Plaza, J., Pujadas, M., Gómez-Moreno, F. J., Sánchez, M., and Artíñano, B.: Mass size distributions of soluble sulfate,
756 nitrate and ammonium in the Madrid urban aerosol, Atmos Environ, 45, 4966–4976, 2011.

757 Podolske, J. R., Sachse, G. W., and Diskin, G. S.: Calibration and data retrieval algorithms for the NASA
758 Langley/Ames Diode Laser Hygrometer for the NASA Transport and Chemical Evolution over the Pacific (TRACE-
759 P) mission, Journal of Geophysical Research: Atmospheres, 108, https://doi.org/10.1029/2002jd003156, 2003.

760 Pye, H. O. T., Chan, A. W. H., Barkley, M. P., and Seinfeld, J. H.: Global modeling of organic aerosol: The importance
761 of reactive nitrogen (NOx and NO3), Atmos Chem Phys, 10, 11261–11276, https://doi.org/10.5194/acp-10-11261-
762 2010, 2010.

763 Ramnarine, E., Kodros, J. K., Hodshire, A. L., Lonsdale, C. R., Alvarado, M. J., and Pierce, J. R.: Effects of near-
764 source coagulation of biomass burning aerosols on global predictions of aerosol size distributions and implications
765 for aerosol radiative effects, Atmos Chem Phys, 19, 6561–6577, https://doi.org/10.5194/acp-19-6561-2019, 2019.

766 Reid, J. S., Eck, T. F., Christopher, S. A., Koppman, R., Dubovik, O., Eleuterio, D. P., Holben, B. N., Reid, E. A., and
767 Zhang, J.: A review of biomass burning emissions part III: Intensive optical properties of biomass burning particles,
768 Atmos Chem Phys, 5, 827–849, https://doi.org/10.5194/acp-5-827-2005, 2005.

769 Remoundaki, E., Kassomenos, P., Mantas, E., Mihalopoulos, N., and Tsezos, M.: Composition and mass closure of
770 PM2.5 in urban environment (Athens, Greece), Aerosol Air Qual Res, 13, 72–82,
771 https://doi.org/10.4209/aaqr.2012.03.0054, 2013.

Reutter, P., Su, H., Trentmann, J., Simmel, M., Rose, D., Gunthe, S. S., Wernli, H., Andreae, M. O., and Pöschl, U.: Aerosol- and updraft-limited regimes of cloud droplet formation: Influence of particle number, size and hygroscopicity on the activation of cloud condensation nuclei (CCN), Atmos Chem Phys, 9, 7067–7080, https://doi.org/10.5194/acp-9-7067-2009, 2009.

Rissler, J., Vestin, A., Swietlicki, E., Fisch, G., Zhou, J., Artaxo, P., and Andreae, M. O.: Size distribution and hygroscopic properties of aerosol particles from dry-season biomass burning in Amazonia, Atmos Chem Phys, 6, 471–491, https://doi.org/10.5194/acp-6-471-2006, 2006.

Rodríguez, S., Van Dingenen, R., Putaud, J. P., Dell'Acqua, A., Pey, J., Querol, X., Alastuey, A., Chenery, S., Ho, K. F., Harrison, R., Tardivo, R., Scarnato, B., and Gemelli, V.: A study on the relationship between mass concentrations, chemistry and number size distribution of urban fine aerosols in Milan, Barcelona and London, Atmos Chem Phys, 7, 2217–2232, https://doi.org/10.5194/acp-7-2217-2007, 2007.

Ruijrok, W., Davidson, C. I., and Nicholson, K. W.: Dry deposition of particles, Tellus B, 47, 587–601, https://doi.org/10.1034/j.1600-0889.47.issue5.6.x, 1995.

Sakamoto, K. M., Laing, J. R., Stevens, R. G., Jaffe, D. A., and Pierce, J. R.: The evolution of biomass-burning aerosol size distributions due to coagulation: Dependence on fire and meteorological details and parameterization, Atmos Chem Phys, 16, 7709–7724, https://doi.org/10.5194/acp-16-7709-2016, 2016.

Sawamura, P., Moore, H. R., Burton, P. S., Chemyakin, E., Müller, D., Kolgotin, A., Ferrare, A. R., Hostetler, A. C., Ziemba, D. L., Beyersdorf, J. A., and Anderson, E. B.: HSRL-2 aerosol optical measurements and microphysical retrievals vs. airborne in situ measurements during DISCOVER-AQ 2013: An intercomparison study, Atmos Chem Phys, 17, 7229–7243, https://doi.org/10.5194/acp-17-7229-2017, 2017.

Schubert, S. D., Rood, R. B., and Pfaendtner, J.: An Assimilated Dataset for Earth Science Applications, Bull Am Meteorol Soc, 74, 2331–2342, https://doi.org/10.1175/1520-0477(1993)074<2331:AADFES>2.0.CO;2, 1993.

Schwarz, J. P., Gao, R. S., Fahey, D. W., Thomson, D. S., Watts, L. A., Wilson, J. C., Reeves, J. M., Darbeheshti, M., Baumgardner, D. G., and Kok, G. L.: Single-particle measurements of midlatitude black carbon and light-scattering aerosols from the boundary layer to the lower stratosphere, Journal of Geophysical Research: Atmospheres, 111, 2006.

Seinfeld, J. H. and Pandis, S. N.: Atmospheric Chemistry and Physics, Third., John Wiley, New York, 2016.

Shah, V., Jacob, D. J., Moch, J. M., Wang, X., and Zhai, S.: Global modeling of cloud water acidity, precipitation acidity, and acid inputs to ecosystems, Atmos Chem Phys, 20, 12223–12245, https://doi.org/10.5194/acp-20-12223-2020, 2020.

Snider, G., Weagle, C. L., Murdymootoo, K. K., Ring, A., Ritchie, Y., Stone, E., Walsh, A., Akoshile, C., Anh, N. X., Balasubramanian, R., Brook, J., Qonitan, F. D., Dong, J., Griffith, D., He, K., Holben, B. N., Kahn, R., Lagrosas, N., Lestari, P., Ma, Z., Misra, A., Norford, L. K., Quel, E. J., Salam, A., Schichtel, B., Segev, L., Tripathi, S., Wang, C., Yu, C., Zhang, Q., Zhang, Y., Brauer, M., Cohen, A., Gibson, M. D., Liu, Y., Martins, J. V., Rudich, Y., and Martin,

R. V.: Variation in global chemical composition of PM2.5: emerging results from SPARTAN, Atmos Chem Phys, 16, 9629–9653, https://doi.org/10.5194/acp-16-9629-2016, 2016.

Sullivan, A. P., Guo, H., Schroder, J. C., Campuzano-Jost, P., Jimenez, J. L., Campos, T., Shah, V., Jaeglé, L., Lee, B. H., Lopez-Hilfiker, F. D., Thornton, J. A., Brown, S. S., and Weber, R. J.: Biomass Burning Markers and Residential Burning in the WINTER Aircraft Campaign, Journal of Geophysical Research: Atmospheres, 124, 1846–1861, https://doi.org/10.1029/2017JD028153, 2019.

Sun, J., Zhang, Q., Canagaratna, M. R., Zhang, Y., Ng, N. L., Sun, Y., Jayne, J. T., Zhang, X., Zhang, X., and Worsnop, D. R.: Corrigendum to "Highly time- and size-resolved characterization of submicron aerosol particles in Beijing using an Aerodyne Aerosol Mass Spectrometer" [Atmos. Environ. 44 (2010) 131-140], Atmos Environ, 47, 570, https://doi.org/10.1016/j.atmosenv.2010.01.023, 2012.

Sun, Y. L., Zhang, Q., Schwab, J. J., Chen, W. N., Bae, M. S., Lin, Y. C., Hung, H. M., and Demerjian, K. L.: A case study of aerosol processing and evolution in summer in New York City, Atmos Chem Phys, 11, 12737–12750, https://doi.org/10.5194/acp-11-12737-2011, 2011.

Szopa, S., Balkanski, Y., Schulz, M., Bekki, S., Cugnet, D., Fortems-Cheiney, A., Turquety, S., Cozic, A., Déandreis, C., Hauglustaine, D., Idelkadi, A., Lathière, J., Lefevre, F., Marchand, M., Vuolo, R., Yan, N., and Dufresne, J. L.: Aerosol and ozone changes as forcing for climate evolution between 1850 and 2100, Clim Dyn, 40, 2223–2250, https://doi.org/10.1007/s00382-012-1408-y, 2013.

Tian, P., Liu, D., Huang, M., Liu, Q., Zhao, D., Ran, L., Deng, Z., Wu, Y., Fu, S., Bi, K., Gao, Q., He, H., Xue, H., and Ding, D.: The evolution of an aerosol event observed from aircraft in Beijing: An insight into regional pollution transport, Atmos Environ, 206, 11–20, https://doi.org/10.1016/j.atmosenv.2019.02.005, 2019.

Timonen, H., Aurela, M., Carbone, S., Saarnio, K., Saarikoski, S., Mäkelä, T., Kulmala, M., Kerminen, V.-M., Worsnop, D. R., and Hillamo, R.: High time-resolution chemical characterization of the water-soluble fraction of ambient aerosols with PILS-TOC-IC and AMS, Atmos Meas Tech, 3, 1063–1074, 2010.

Twomey, S.: Pollution and the Planetary Albedo, Atmos Environ, 41, 120–125, https://doi.org/10.1016/j.atmosenv.2007.10.062, 2007.

Wang, J., Xu, X., Ding, S., Zeng, J., Spurr, R., Liu, X., Chance, K., and Mishchenko, M.: A numerical testbed for remote sensing of aerosols, and its demonstration for evaluating retrieval synergy from a geostationary satellite constellation of GEO-CAPE and GOES-R, J Quant Spectrosc Radiat Transf, 146, 510–528, https://doi.org/10.1016/j.jqsrt.2014.03.020, 2014a.

Wang, Q., Jacob, D. J., Spackman, J. R., Perring, A. E., Schwarz, J. P., Moteki, N., Marais, E. A., Ge, C., Wang, J., and Barrett, S. R. H.: Global budget and radiative forcing of black carbon aerosol: Constraints from pole-to-pole (HIPPO) observations across the Pacific, J Geophys Res, 119, 195–206, https://doi.org/10.1002/2013JD020824, 2014b.

838 Wang, Y., Jacob, D. J., and Logan, J. A.: Global simulation of tropospheric O3-NOx-hydrocarbon chemistry - 1.
839 Model formulation, Journal of Geophysical Research: Atmospheres, 103, 10713–10725,
840 https://doi.org/10.1029/98jd00158, 1998.

841 Weagle, C. L., Snider, G., Li, C., Van Donkelaar, A., Philip, S., Bissonnette, P., Burke, J., Jackson, J., Latimer, R.,
842 Stone, E., Abboud, I., Akoshile, C., Anh, N. X., Brook, J. R., Cohen, A., Dong, J., Gibson, M. D., Griffith, D., He, K.
843 B., Holben, B. N., Kahn, R., Keller, C. A., Kim, J. S., Lagrosas, N., Lestari, P., Khian, Y. L., Liu, Y., Marais, E. A.,
844 Martins, J. V., Misra, A., Muliane, U., Pratiwi, R., Quel, E. J., Salam, A., Segev, L., Tripathi, S. N., Wang, C., Zhang,
845 Q., Brauer, M., Rudich, Y., and Martin, R. V.: Global Sources of Fine Particulate Matter: Interpretation of PM2.5
846 Chemical Composition Observed by SPARTAN using a Global Chemical Transport Model, Environ Sci Technol, 52,
847 11670–11681, https://doi.org/10.1021/acs.est.8b01658, 2018.

848 Weinheimer, A. J., Walega, J. G., Ridley, B. A., Sachse, G. W., Anderson, B. E., and Collins Jr, J. E.: Stratospheric
849 NOy measurements on the NASA DC-8 during AASE II, Geophys Res Lett, 20, 2563–2566, 1993.

850 Weng, H., Lin, J., Martin, R., Millet, D. B., Jaeglé, L., Ridley, D., Keller, C., Li, C., Du, M., and Meng, J.: Global
851 high-resolution emissions of soil NOx, sea salt aerosols, and biogenic volatile organic compounds, Sci Data, 7, 1–15,
852 https://doi.org/10.1038/s41597-020-0488-5, 2020.

853 Van Der Werf, G. R., Randerson, J. T., Giglio, L., Van Leeuwen, T. T., Chen, Y., Rogers, B. M., Mu, M., Van Marle,
854 M. J. E., Morton, D. C., Collatz, G. J., Yokelson, R. J., and Kasibhatla, P. S.: Global fire emissions estimates during
855 1997-2016, Earth Syst Sci Data, 9, 697–720, https://doi.org/10.5194/essd-9-697-2017, 2017.

856 Westervelt, D. M., Pierce, J. R., Riipinen, I., Trivitayanurak, W., Hamed, A., Kulmala, M., Laaksonen, A., Decesari,
857 S., and Adams, P. J.: Formation and growth of nucleated particles into cloud condensation nuclei: Model-measurement
858 comparison, Atmos Chem Phys, 13, 7645–7663, https://doi.org/10.5194/acp-13-7645-2013, 2013.

859 Whitey, K. T.: The physical characteristics of sulfur aerosols, in: Atmospheric Environment, vol. 41, Elsevier, 25–49,
860 https://doi.org/10.1016/j.atmosenv.2007.10.057, 1978.

861 Yu, F. and Luo, G.: Simulation of particle size distribution with a global aerosol model: Contribution of nucleation to
862 aerosol and CCN number concentrations, Atmos Chem Phys, 9, 7691–7710, https://doi.org/10.5194/acp-9-7691-2009,
863 2009.

864 Yue, D. L., Hu, M., Wu, Z. J., Guo, S., Wen, M. T., Nowak, A., Wehner, B., Wiedensohler, A., Takegawa, N., and
865 Kondo, Y.: Variation of particle number size distributions and chemical compositions at the urban and downwind
866 regional sites in the Pearl River Delta during summertime pollution episodes, Atmos Chem Phys, 10, 9431–9439,
867 2010.

868 Zender, C. S., Bian, H., and Newman, D.: Mineral Dust Entrainment and Deposition (DEAD) model: Description and
869 1990s dust climatology, Journal of Geophysical Research: Atmospheres, 108, https://doi.org/10.1029/2002jd002775,
870 2003.

Zhai, S., Jacob, D., Brewer, J., Li, K., Moch, J., Kim, J., Lee, S., Lim, H., Lee, H. C., Kuk, S. K., Park, R., Jeong, J., Wang, X., Liu, P., Luo, G., Yu, F., Meng, J., Martin, R., Travis, K., Hair, J., Anderson, B., Dibb, J., Jimenez, J., Campuzano-Jost, P., Nault, B., Woo, J.-H., Kim, Y., Zhang, Q., and Liao, H.: Interpretation of geostationary satellite aerosol optical depth (AOD) over East Asia in relation to fine particulate matter (PM2.5): insights from the KORUS-AQ aircraft campaign and seasonality, Atmos Chem Phys, 1–23, https://doi.org/10.5194/acp-2021-413, 2021.

Zhang, L., Kok, J. F., Henze, D. K., Li, Q., and Zhao, C.: Improving simulations of fine dust surface concentrations over the western United States by optimizing the particle size distribution, Geophys Res Lett, 40, 3270–3275, https://doi.org/10.1002/grl.50591, 2013.